# FINAL REPORT

## Modeling Buried Target Acoustic Response by Component

SERDP Project MR-2324

NOVEMBER 2014

Lane Owsley
Aubrey España
**University of Washington**

*Distribution Statement A*
*This document has been cleared for public release*

SERDP
DOD ▪ EPA ▪ DOE

This report was prepared under contract to the Department of Defense Strategic Environmental Research and Development Program (SERDP). The publication of this report does not indicate endorsement by the Department of Defense, nor should the contents be construed as reflecting the official policy or position of the Department of Defense. Reference herein to any specific commercial product, process, or service by trade name, trademark, manufacturer, or otherwise, does not necessarily constitute or imply its endorsement, recommendation, or favoring by the Department of Defense.

# REPORT DOCUMENTATION PAGE

*Form Approved*
*OMB No. 0704-0188*

Public reporting burden for this collection of information is estimated to average 1 hour per response, including the time for reviewing instructions, searching existing data sources, gathering and maintaining the data needed, and completing and reviewing this collection of information. Send comments regarding this burden estimate or any other aspect of this collection of information, including suggestions for reducing this burden to Department of Defense, Washington Headquarters Services, Directorate for Information Operations and Reports (0704-0188), 1215 Jefferson Davis Highway, Suite 1204, Arlington, VA 22202-4302. Respondents should be aware that notwithstanding any other provision of law, no person shall be subject to any penalty for failing to comply with a collection of information if it does not display a currently valid OMB control number. **PLEASE DO NOT RETURN YOUR FORM TO THE ABOVE ADDRESS.**

**1. REPORT DATE** *(DD-MM-YYYY)*
02/09/2015

**2. REPORT TYPE**
Final Technical

**3. DATES COVERED** *(From - To)*
04/16/2013 – 01/15/2015

**4. TITLE AND SUBTITLE**
Modeling Buried Target Acoustic Response by Component

**5a. CONTRACT NUMBER**
W912HQ-13-C-0023

**5b. GRANT NUMBER**

**5c. PROGRAM ELEMENT NUMBER**

**6. AUTHOR(S)**
Lane Owsley, Ph.D.

**5d. PROJECT NUMBER**

**5e. TASK NUMBER**

**5f. WORK UNIT NUMBER**

**7. PERFORMING ORGANIZATION NAME(S) AND ADDRESS(ES)**
University of Washington – Applied Physics Laboratory
4333 Brooklyn Avenue NE
Seattle, WA 98105-6613

**8. PERFORMING ORGANIZATION REPORT NUMBER**

**9. SPONSORING / MONITORING AGENCY NAME(S) AND ADDRESS(ES)**
SERDP PROGRAM OFFICE
HERB NELSON
4800 MARK CENTER DRIVE, SUITE 17D08
ALEXANDRIA VA 22350-3600

**10. SPONSOR/MONITOR'S ACRONYM(S)**

**11. SPONSOR/MONITOR'S REPORT NUMBER(S)**

**12. DISTRIBUTION / AVAILABILITY STATEMENT**

Distribution Statement A: Approved for public release; distribution is unlimited.

**13. SUPPLEMENTARY NOTES**

**14. ABSTRACT**

Automated detection and identification of abandoned mutitions through sonar interrogation requires that system algorithms be robust to a wide variety of environmental and target conditions. Empirical tests are a crucial part of the verification of robustness, but even more basic is a physically-justified design of the algorithm and feature selection. The proposers are developing a finite element (FE) approach to aid in such an incorporation of the target physics; in this SEED project we will focus on using FE simulations to characterize the effects of target burial state on coupling surfaces and wave travel in the sediment and target itself. This research will provide validity for further development of individual physics component modeling.

**15. SUBJECT TERMS**

| **16. SECURITY CLASSIFICATION OF:** | | | **17. LIMITATION OF ABSTRACT** | **18. NUMBER OF PAGES** | **19a. NAME OF RESPONSIBLE PERSON** |
|---|---|---|---|---|---|
| | | | | | Lane Owsley, Ph.D. |
| **a. REPORT** | **b. ABSTRACT** | **c. THIS PAGE** | UU | 36 | **19b. TELEPHONE NUMBER** *(include area code)* |
| Unclassified | Unclassified | Unclassified | | | 206-685-3592 |

**Standard Form 298 (Rev. 8-98)**
**Prescribed by ANSI Std. Z39.18**

# Contents

**1 Introduction** **2**

**2 Response Component Isolation Approaches** **4**
2.1 Isolation of Features by Coupling Angle 5
2.2 Isolation of Features by Vertical Position 8

**3 Simulations as a function of shell and filler material** **8**

**4 Simulations as a function of burial state** **14**

**5 CSAS Simulations Over a Wide Range of Grazing Angle and Environment Properties** **16**

**6 Dissecting the Effects of Multipath** **19**

**7 Implementation of Component Isolation Techniques** **19**

**8 Future Work** **24**

**Appendix A Physics feature Isolation: Specular, Inelastic Fluid-Borne, and Elastic** **30**

**Appendix B Using Table Lookups to Efficiently Simulate Acoustic Responses** **32**

# 1 Introduction

The goal of developing a robust automatic identification system for the scattered acoustic responses from underwater targets like UXOs requires an understanding of the physics underlying those responses. Even if a system trained on observed data performs well in limited field tests, if the underlying feature set cannot be related to the physical structure and behavior of the target then it is impossible to have confidence in the ability to generalize performance estimation to other environments and burial states, target configurations, and non-target clutter.

Much of the state-of-the-art in physical interpretation of the response of complex targets is a result of extensive study of the free-field response of very simple shapes, such as spheres and infinite cylinders, whose physics can be modeled and solved analytically. Although the research on these shapes has resulted in the identification of a wide variety of physical behaviors which contribute to the varying pattern of the scattered response as a function of frequency, source angle, and receiver angle, the observed patterns change significantly as the shapes are modified toward targets of strategic interest. The outcome has been that current systems, even when successful in the field, only use the knowledge gained from analytic studies in a very general sense to inform the selection of feature sets. Still less physics-based and more reliant on empirical studies is our understanding of the effect of such variability sources as burial state on system performance.

Finite element (FE) models have made enormous contributions to the prediction of the physical behavior of a much wider class of structures than can be modeled analytically. The FE approach is to break complex structures down into very small elements whose behavior can be described mathematically, and then simultaneously solve for the response of all such elements to produce the response of the complete complex system. The experiments described in this report use a howitzer-like metal shell with variable filler (shown in Figure 1), but we have modeled much more complicated structures as well. The standard use of FE models is to reproduce the exciting source (such as a sonar pressure wave) as accurately as possible, and then examine the resulting scattered response. Empirical tests have shown a high degree of fidelity to such simulations on the types of targets of interest in UXO detection, which gives us confidence in the value of interpretations based on these simulated responses to drive the creation of automated target identification systems. However, highly accurate simulated responses are by definition as complex as the true response and thus present the same problems of interpretation.

It is the objective of the research discussed in this report to make a different use of FE models by systematically constraining the models and their exciting physics in such a manner as to isolate components of the response and make physical interpretation of these components possible. Considering the problem from this perspective opens up a wide variety of approaches to feature heirarchy. In our previously published work [1], we describe a method for separately modeling the specular, non-specular fluid-borne, and elastic components of the response. In this SEED effort, we have been focusing on further subdividing the elastic response. We looked at two basic approaches: coupling-angle-focused and depth-focused. The former was motivated by ray-theory research that recognizes certain phase-matching conditions are necessary for certain types of fluid-structure coupling, and suggests a direction for isolation and identification of the corresponding scattered-wave features. We have also looked at isolating features by the depth of the target surface on which they couple; this is motivated by the awareness that in the field the targets may be partially buried and thus the ability to characterize the features by depth will be directly relevant.

For comparison, we have also simulated the full-physics responses of the target in various states of burial using approaches that we have previously demonstrated as producing a high degree of fidelity to field-collected data [2] [3]. These results serve as a point of comparison for the depth-based feature isolation just mentioned. This approach is also critical for determining the direction

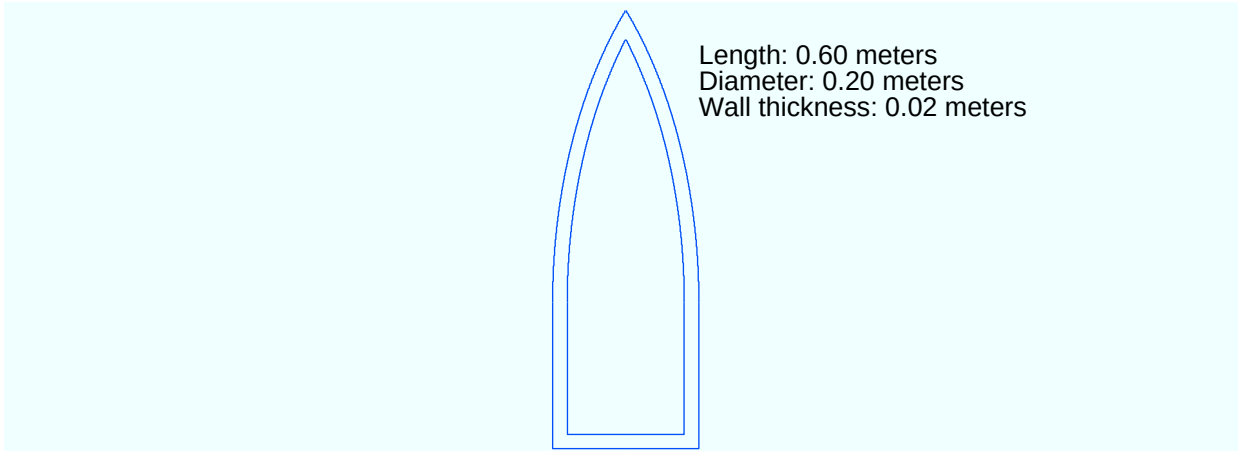


**Figure 1: Geometry of target used in these studies. The shell thickness and composition, as well as the composition of the internal filler, are parameterized and can be modified.**

for future research which must consider the interaction of acoustic paths from both the direct wave and those which reflect off (or travel through) the sediment. Finally, we have performed comparisons of the response for different unclassified fillers. Consideration of multiple fillers is vital, because it allows us to frame the results from the approaches described above so as to avoid making assumptions which are assumed to be universal but are in fact specific to a particular filler type.

The remainder of the report is divided into the following sections:

- A description of the FE component isolation modeling approach which allows us to isolate elastic features in a variety of ways
- Results using the above approach for two region-loading hierarchies:
  - Isolation by coupling angle
  - Isolation by depth location
- Simulations as a function of shell and filler material and the implications for features observed above
- Simulations as a function of burial state, and their use as a framework for analysis of the region-load approach
- CSAS simulations over a wide range of grazing angle and environment properties, thus illustrating the successful merging of two SERDP-funded modeling capabilities.
- Consideration of the effects of multipath on the results of the above studies
- Example of the use of the above approaches in combination to understand the complex scattered return
- Proposed directions for future work

## 2 Response Component Isolation Approaches

The goal of the FE modeling approach we are taking at APL-UW is to break down the complex scattered responses of targets of interest by manipulating the physics in a variety of ways so as to produce simpler responses that allow us to relate the observed farfield response to particular physical mechanisms and target components. This enables us to understand field-collected data and ultimately to develop physically-motivated feature sets for automatic target identification, characterize the effects of environment and burial on those feature sets, and improve system performance. In previous work (summarized in Appendix A of this report), we demonstrated a method for separately modeling the target's inelastic and elastic response, decomposing the inelastic response even further into specular and fluid-borne interface-guided components. In the SEED effort reported on here, one of our key research goals is to explore methods of further breaking down the elastic portion of the response. As described in Appendix A, a model of the complete physics of the target includes the explicit statement that the fluid surrounding a solid target exerts a force on that solid which is a function of the total fluid pressure $p_{tot}$:

$$\mathbf{F} = -p_{tot}\mathbf{N}, \tag{1}$$

where $\mathbf{N}$ is the normal vector of the solid surface and we recognize that all terms are functions of position and time. Defining $p_{inc}$ as the incident pressure wave in the absence of a target and recognizing that the total pressure can be represented as the sum of the incident and scattered pressure:

$$p_{tot} = p_{inc} + p_{scat}, \tag{2}$$

as a first approach we are neglecting the effects of the scattered response and simply modeling the effects of the load of the incident pressure on the target:

$$\mathbf{F} = -p_{inc}\mathbf{N}. \tag{3}$$

By investigating the response due to this fluid load alone, we are in effect "shaking" the target directly and isolating the elastic response without ever simulating the incident wave in the acoustic domain.

The approximation of the total pressure field load as that of the incident pressure field is more problematic in some places than others. An obvious case is the fluid region at the rear of the target (relative to the source), where the effects of the incident pressure are greatly reduced (and in any case not correctly modeled) by $p_{inc}$. As a result, in the proposal for the completed SEED work we discussed modeling the scattered effects of the load only on the front of the target. At the time the proposal was written, this required decomposing the representation of the pressure load into the modal representation of the axiscat modeling technique we were using to represent the target [4]. However, recent advances in this modeling approach by Marten Nijhof at TNO and Aubrey España (a performer in the current effort) at APL-UW [5] allow us much more flexibility in customizing the loading region, which means that we can not only more accurately model effects of target shadowing on the fluid loading, but also limit the incident forces using a wide variety of methodologies which enable us to pursue the component isolation approaches which are the ultimate goal of this research.

The Nijhof method, which is more fully described in Appendix B of this report and derived from a modeling technique originally introduced by Zampolli [4, 6], involves a precalculation of the responses due to loading the individual FE gauss points in isolation. Storing these results in a large (greater than one terabyte) table requires a week of computer time on a dedicated fast computer, but afterwards this table can be used to quickly simulate the response for a wide variety

of loading conditions. In Section 4 we will discuss using these tables to directly simulate various states of burial for the complete physics; in the current section we are interested in isolating the elastic response for a load applied to a small portion of the target. This involves applying a spatial mask to the pressure load described in Equation 3.

To get a feel for the use of masks in isolating return features, consider the example masks shown in Figure 2 for an axisymmetric pointed-endcap filled-shell target on which we have focused much of our modeling in this effort. The subfigures show a number of masks which enforce different constraints on the region to which the incident load will be applied. Figure 2a constrains the load to be applied only to the portion of the target not in the shadow. Figure 2b restricts the incident energy based on vertical position, which is useful in considering the effects of burial. Figure 2c masks the endcap, which allows us to focus on coupling into the surface parallel to the axis. Figure 2d restricts the coupling angle (this will be discussed further in Section 2.1) between the source direction and the target surface normal to a band of angles, which is of value in isolating physical behaviors of different phase velocities. Using various combinations of these and similar masks allows us to study and break down the elastic response according to various hierarchies; the mask created by combining all the above masks is shown in Figure 2f. In the next two subsections, we discuss two hierarchies we are investigating using this approach. Ultimately these approaches will be combined in Section 7 to help isolate the various components making up the response of a fully buried target.

Before delving into examples of using loading masks to isolate features in Subsections 2.1 and 2.2, it is important for us to note that the masking approach taken in the SEED effort is only one method of simplifying the features under the framework we have developed; there are many other physically-motivated isolation approaches that would be of great interest in simplifying the elastic portion of the scattered return. In Section 8 of this report, we propose a future direction of work that restricts the phases and angles of displacement within the target to correspond with known wave types. This will allow us to leverage a much wider range of physics research into our understanding of the robustness of returns to variation due to burial and material.

### 2.1 Isolation of Features by Coupling Angle

Ray theory [7, 8, 9] has been used for decades as an approach to prediction of certain features of the scattered return from cylindrical and spherical targets. Underlying ray theory is the idea that, for sufficiently high-frequency incident waves, the phase-matching conditions between the fluid-borne behavior and solid-surface behavior restrict the range of angles between the source direction and the surface normal at which contstructive interaction will occur. Outside of this range of angles, much less energy will be transferred from the fluid to the solid (or back again). Ray theory idealizes this range as a single angle $\theta_l$ which is a function of the relative wave travel speeds in the liquid ($c$) and the solid ($c_l$):

$$\theta_l = sin^{-1}(\frac{c}{c_l}) \tag{4}$$

The value of $c_l$ is, in turn, a function of the particular wave behavior of interest and the thickness and composition of the solid (and, depending on its thickness, the composition of the filler). For simple shapes, ray theory can be used to trace a path through the fluid, along the solid (with appropriate refraction and reflection angles) and back out into the fluid and to the receiver in such a manner as to be notably consistent with empirically collected data. It should be emphasized again that the research goal of this SEED effort is *not* to duplicate the results of ray theory or any other approach that relies on the target being simple enough to allow for such mathematical analysis. However, the success of ray theory shows the importance of features which can be characterized

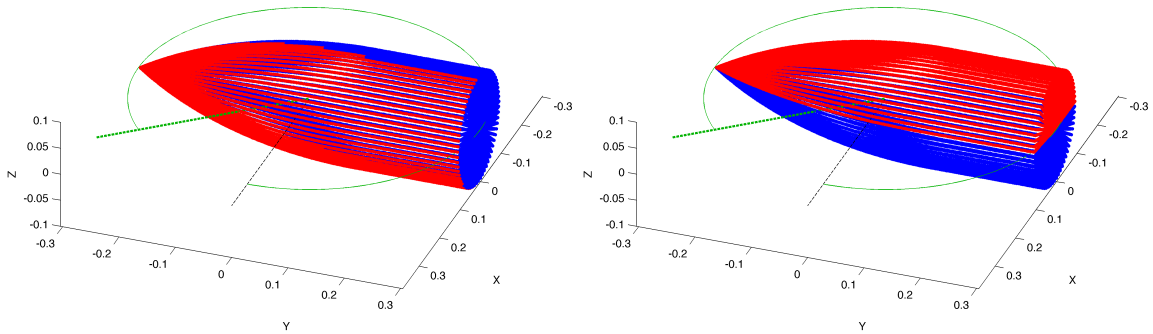


(a) Masking by acoustic shadow




(b) Masking out buried region

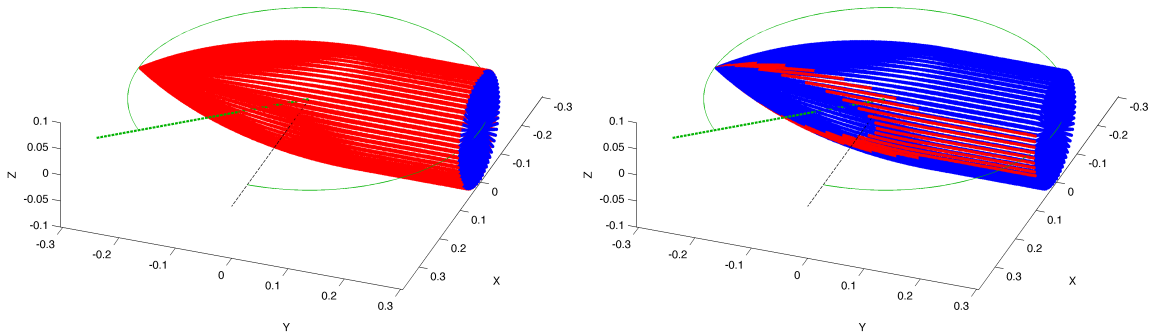


(c) Masking flat endcap




(d) Masking to limit coupling angles

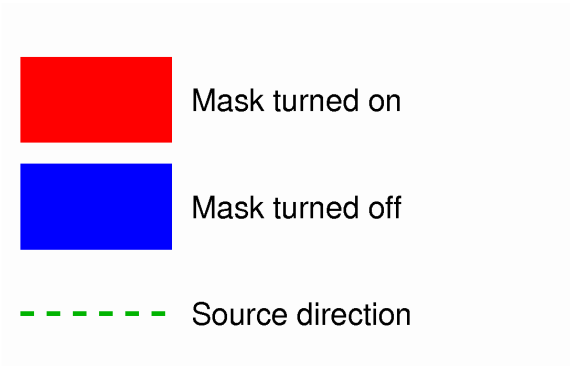


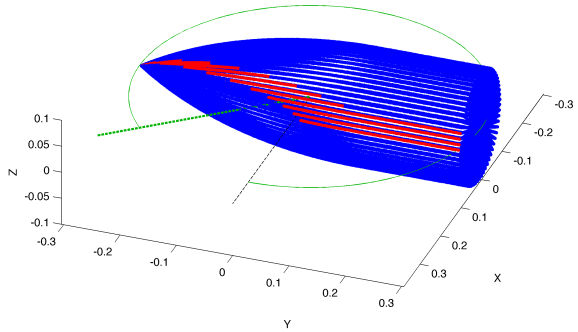


(f) Combined mask

**Figure 2: An example of physics simplification by use of masks on the excitation of gauss points. The masks in Figures 2a-2d are combined to produce the overall mask in Figure 2f.**

by a fluid/solid coupling angle and this result motivates our first approach to breaking down the complete response by physical mechanism. Figure 3 presents a number of masks which allow us to load the target to isolate the response due to a wave type that has a particular phase velocity (and thus a particular coupling angle). The left column of Figure 3 is for the coupling angle range between 45°and 55°; the right column is for the coupling range between 15°and 20°. It can be seen that the masks change, as would be expected, as the angle of the target changes with respect to the source. We can multiply these masks with other masks (as is done with the mask in Figure 2d) to produce a combined mask which isolates the loading region to reflect other desired physics characteristics as well. Figure 4 shows the monostatic farfield returns for various coupling bands as a function of source azimuth and frequency[1].

To validate the physical meaning of this representation of the response, we consider results from analytic acoustic theory. Although the major goal of this approach is a physics-based feature identification method that does not rely on pre-knowledge of the particular physical mechanisms or their relevant parameters, in this research phase of the project it is crucial for validation of our approach that our observed results match with response components that are understood from theoretical analysis. It has been shown that leaky helical rays can lead to enhancements of the observed backscattering from truncated cylinders and shells [3, 7, 10]. These rays are launched at an angle $\theta_l$ defined by Equation 4, where $c_l$ is the phase speed of the leaky wave of type $l$. Two types of leaky helical waves are investigated here, namely compressional and shear. For compressional waves, $c_l$ is defined by the phase speed of compressional waves in a flat plate, denoted $c_p$, and calculated using the Young's modulus and Poisson's ratio for the elastic material. For shear waves, the appropriate $c_l$ is given by the shear speed of the shell material. Using the material properties for aluminum cited by Williams [2], these coupling angles are 15.4 degrees for compressional and 27.7 degrees for shear waves. Figure 4a shows the results of restricting the coupling region to $14° < \theta_l < 18°$, while Figure 4b restricts the coupling region to $25° < \theta_l < 30°$. For a cylinder or cylindrical shell, when the source angle is greater than $\theta_l$, there is no longer any energy coupled into the target. For the shell studied here, however, the pointed nose is such that it is possible to couple energy into these modes beyond the $\theta_l$ cutoff angle. It is important to note that there are other types of modes that can presumably be excited in these coupling regions (combinations of azimuthal and axial modes for example), so this is only meant to reduce the number of enhancements seen the the full response, thus making the helical modes more visible. In these results we have restricted the coupling region for sound onto the shell surface, but are still looking at the full scattered field. More recently, we have added the capability to restrict the de-coupling region of sound on the target as it travels from the solid surface back out into the water column which can serve to isolate the helical modes even more. That being said, there are still observable differences between (a) and (b) that hint at the distinction of compressional vs. shear modes. Further confirmation is gained through the calculation of the coupling loci, or specific angle-frequency pairs in which sound can couple into these helical modes, a method that is discussed in detail in *JASA* by España [3]. Calculation of these coupling loci allows us to confirm the isolation of helical modes, specifically in Figure 4a the locations marked by the red dots at 14 kHz and 17 kHz, (13 deg.) are compressional modes. Similarily in Figure 4b the red dots at 10, 11, and 13 kHz (25 deg.), and 15 and 17 kHz (30 deg.) are shear modes.

[1]The returns shown in Figure 4 have been normalized to show the returned energy conditioned by angle. This is because, as shown in Figure 3, the masks utilized vary by source angle. Since in the FE modeling procedure this mask is applied to the gauss points, different points are active at each angle. The narrow range of angles can result in a small number of gauss points, and particular shifts in source angle that correspond to changes in gauss point activation produce large jumps in relative return magnitude. In subsequent experiments we have increased the number of gauss points to reduce these artifacts.

In addition to the helical modes, Figure 4 shows that there are a number of bright resonances, such as those at approximately 2.15 kHz, 3.4 kHz and 4.25 kHz, that appear to be excited over all four of these different angular coupling regions in (a)-(d). A similar analysis can be done to calculate the coupling loci for other types of modes. Specifically, an axial mode is excited when the projection of the incident field down the axis of the shell has an integer number of half-wavelengths. Similarly, an azimuthal mode is excited when the same condition is met around the shell's circumference. A good visual tool that can help identify these modes is shown in Figure 5(a-c), which plot the real part of the pressure field just outside of the shell surface (Subfigures d-f show more complicated behavior that will be discussed in the Future Work section of this report.) The resonance at 2.15 kHz, -59 deg. is shown in Figure 5a and turns out to be the first order azimuthal mode, also called a bending mode. Similarly, the resonances at (b) 3.4 kHz, 0 deg. and (c) 4.25 kHz, -31 deg. have both met the trace-matching condition for higher order azimuthal modes (specifically of order $n$=3, or 3 half-wavelengths around the circumference), but they each have a different axial dependence. While the resonance in (b) has no axial dependence, the resonance in (c) has met the condition for a first order axial mode (one half-wavelength down the length of the shell). These types of modes are important since they can be excited over a wide range of coupling conditions and have the potential of being robust enough to survive in a number of different environments and burial conditions.

### 2.2 Isolation of Features by Vertical Position

Section 2.1 described an approach to dividing components of the observed response based on the physics of energy transfer within the target; in the case actually described we were grouping components according to the surface wave speed and hence the corresponding coupling angle. This meant that the region to which a load was applied could in theory be anywhere on the target surface, as long as it met the coupling conditions. In some sense the approach described in the current section is the opposite approach: we are basing the region load subdivisions on restrictions imposed by the surrounding environment. In particular, we are taking an approach that will be useful in considering the way burial affects elastic energy transfer. The loading masks shown in Figure 6 are bounded by vertical position (for a target with an axis parallel to the sediment layer). This allows us to observe the response for energy coupled from the fluid at particular depth bands and make inferences about the impact of sediment covering these regions. Figure 7 shows the farfield pressures resulting from these simulations. An important observation here is that the azimuthal and axial modes identified in the previous section (2.15 kHz, 3.4 kHz, and 4.25 kHz) are strongly excited when only the top of the shell is loaded (Figure 7d). One can imagine a situation where the shell could be partially buried in a highly attenuating sediment. Even though the sound incident on the buried portion of the shell is highly damped, these resonances will still be excited and radiate due to the top part of the shell still being exposed in the water column. Another important note is that in Figure 7c and d, the enhancements seen at -50 deg for frequencies above 6 kHz turn out to be associated with the particular type of filler inside of the shell, which will be discussed further in Section 3.

## 3 Simulations as a function of shell and filler material

Thus far we have illustrated how the technique of region-loading a target can isolate particular components of the target physics, specifically where and how the sound couples onto the target, and in some situations, the mechanics as to how it travels down the elastic structure driving a resonance. However, a sufficient understanding of the target response is not always realized simply by knowing

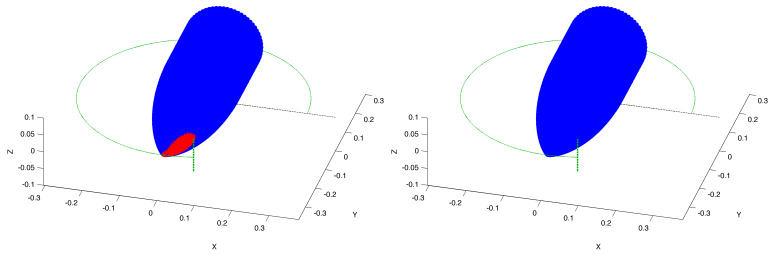

(a) Source azimuth -75°



(b) Source azimuth -75°

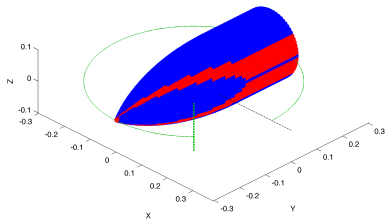

(c) Source azimuth -45°

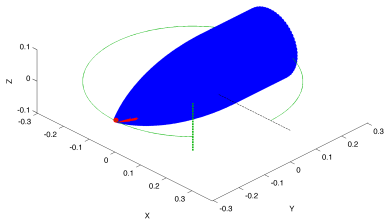

(d) Source azimuth -45°

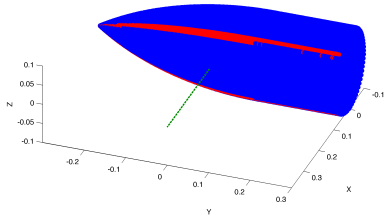

(e) Source azimuth 0°(broadside)

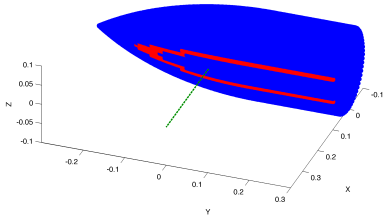

(f) Source azimuth 0°(broadside)

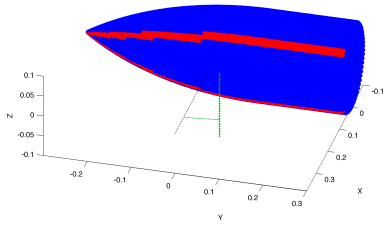

(g) Source azimuth 15°

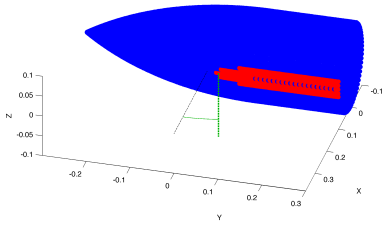

(h) Source azimuth 15°

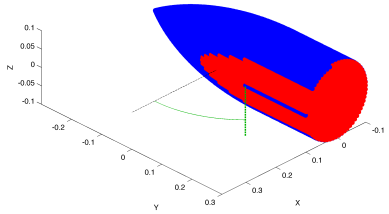

(i) Source azimuth 45°

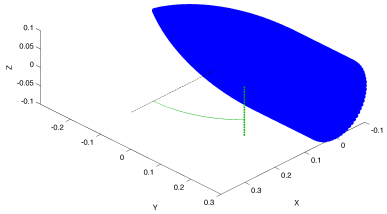

(j) Source azimuth 45°

**Figure 3: Loading regions associated with different coupling angle limits; the left column is limited to coupling angles between 45°and 55°; the right column is limited to coupling angles between 15°and 20°. These masks could be used as the mask in Figure 2d.**

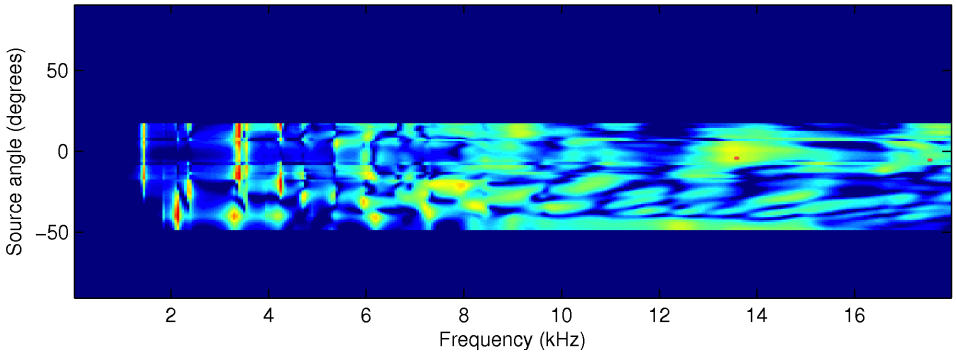


(a) Loading region restricted to coupling angle range 14°to 18°

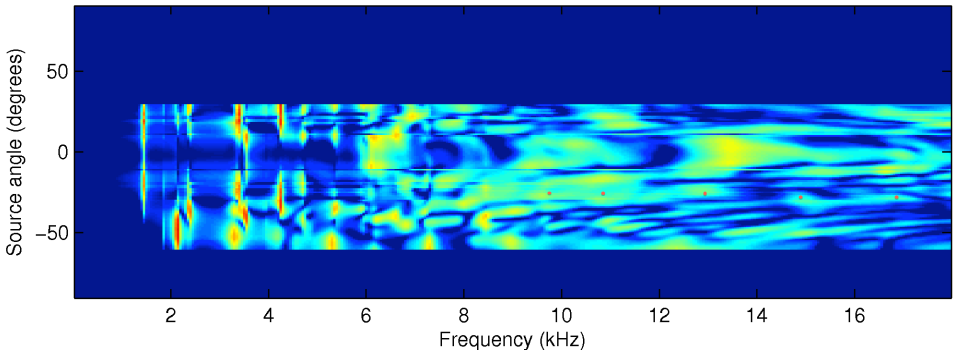


(b) Loading region restricted to coupling angle range 25°to 30°

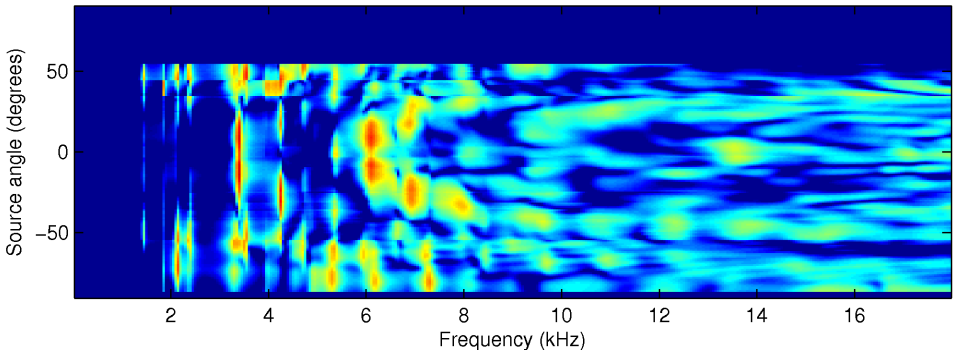


(c) Loading region restricted to coupling angle range 45°to 55°

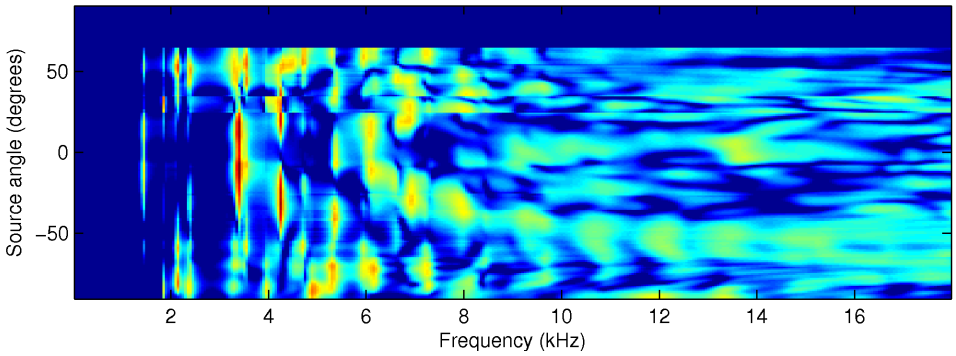


(d) Loading region restricted to coupling angle range 55°to 65°

**Figure 4: Monostatic angle-conditioned farfield elastic response for the pointed-end-cap shell (water-filled) with loading restricted to particular coupling ranges as in Figure 3. For example, the response in Figure 4c corresponds to the left column of Figure 3.**

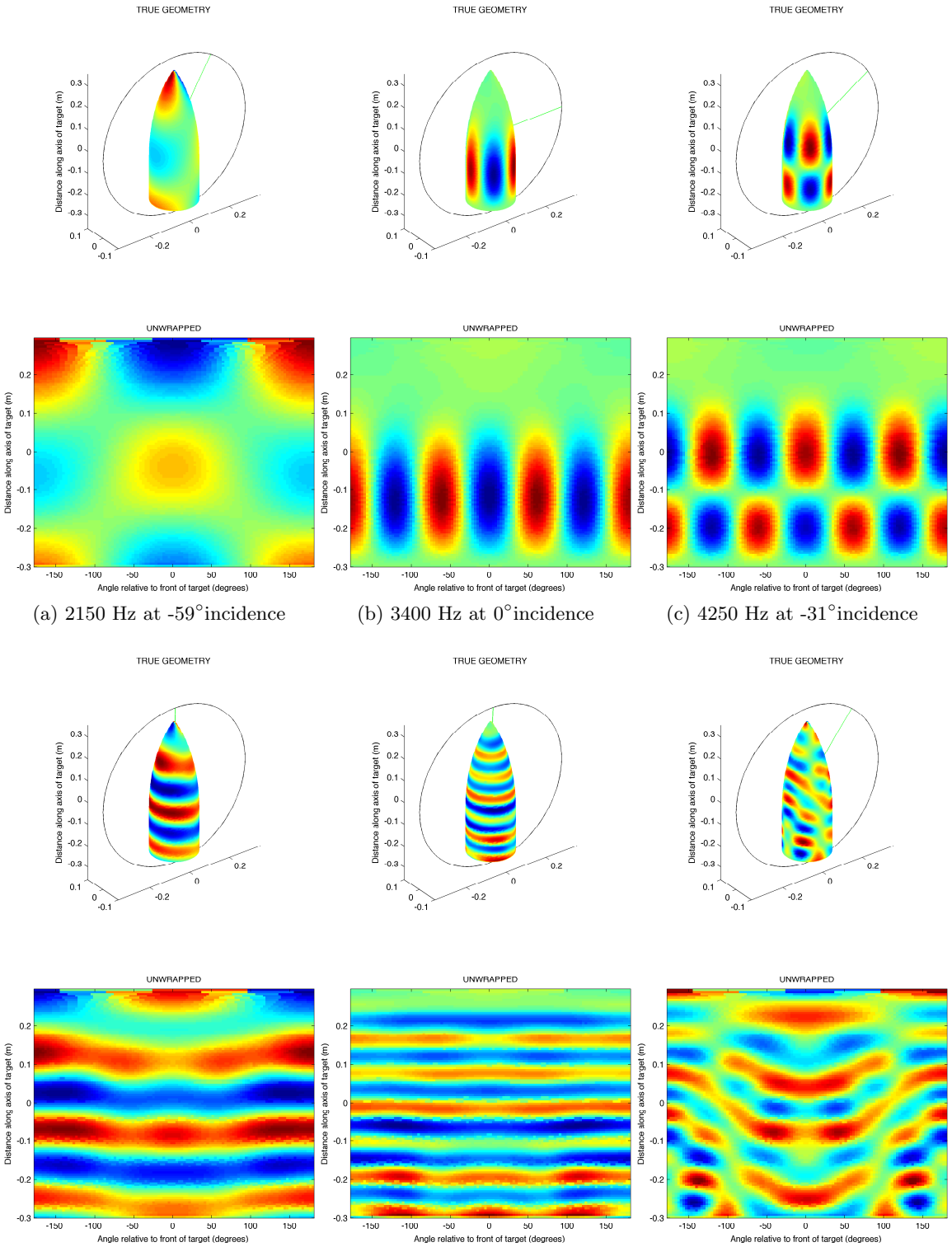


(a) 2150 Hz at -59°incidence (b) 3400 Hz at 0°incidence (c) 4250 Hz at -31°incidence

(d) 6000 Hz at -89°incidence (e) 14750 Hz at -88°incidence (f) 13500 Hz at -51°incidence

**Figure 5: Inspecting the real part of the near-field pressure field (just outside the shell) for features observed in 4. The fields are shown both in true geometry and unwrapped to make visual inspection simpler. This approach allows us to relate the acoustic color feature to the geometry and coupling location.**

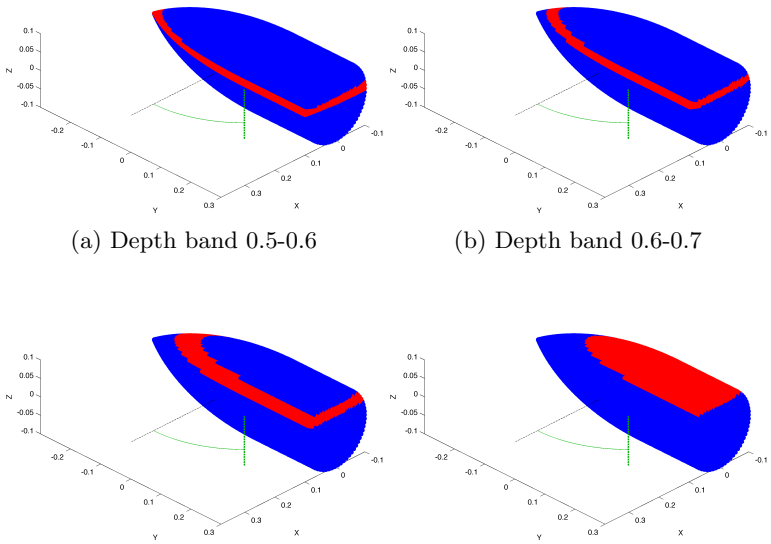

(a) Depth band 0.5-0.6 (b) Depth band 0.6-0.7

(c) Depth band 0.7-0.85 (d) Depth band 0.85-1.00

**Figure 6: Loading regions corresponding to limitations on depth bands (described in units of height from target bottom normalized to target diameter). These masks could be used as the mask in Figure 2d.**

the coupling mechanisms. For this aspect of the research, we look into how the particular shell material and its filler play into the target response. The same pointed-end-cap shell is used for this study. The response for two identically shaped pointed-end-cap shells is investigated, one composed of steel and one of aluminum, and each filled with water and/or air.

The effects of the shell and filler material are best summarized through Figure 8. All of the shells were interrogated in the free field (zero degree grazing angle) with a full plane wave (left-most column) in addition to a fluid load case (right-most column) as discussed in Section 2 which isolates the elastic response of the targets. It is important to note that this type of fluid-only loading is highly advantageous since it removes all of the inelastic response, thus isolating the elastic effects which may be associated with the shell and filler materials. The top row shows the response for the water-filled steel shell, middle row is the water-filled aluminum shell and the bottom row corresponds to the air-filled aluminum shell. Comparison of the top two rows (which only differ in shell material) shows that differences between shell material tend to manifest at and around broadside (0 deg) for this frequency range. This is not surprising since the coupling of sound to shear and longitudinal modes of azimuthally symmetric objects typically occurs in the region from 0-30 degrees, the exact location being dictated by the shear and compressional sound speeds of the shell material and the fulfillment of a trace-matching condition for the projection of the incident wave vector along the target axis [3]. Comparison of the bottom two rows (water versus air filled) reveals that the filler material has a strong effect on the response away from broadside, specifically from +/- 30 deg to +/- 90 deg. The most prominent difference is around +/-50 deg, in which the water-filled shell shows a strong response (especially at -50 deg) while the air-filled does not. This water-filled aluminum shell was the subject of discussion during Sections 2.1 and 2.2. It is important to note that the response of the shell at -50 deg, which is now known to be driven by the filler material, was a feature that could be excited by restricting the loading according to coupling

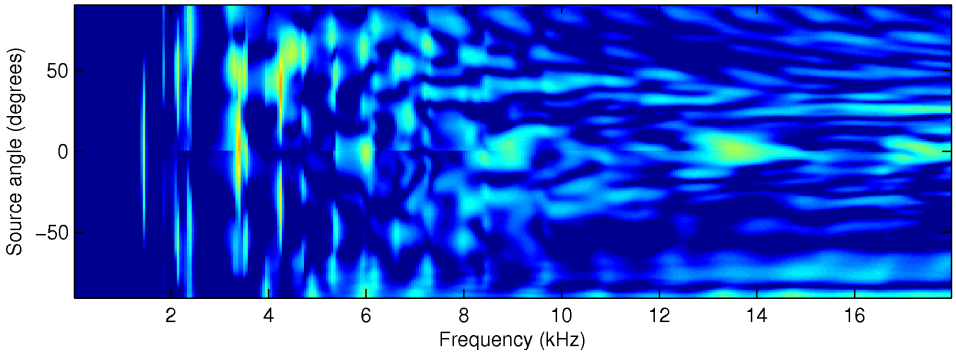


(a) Loading region restricted to depth band 0.5 to 0.6 of diameter

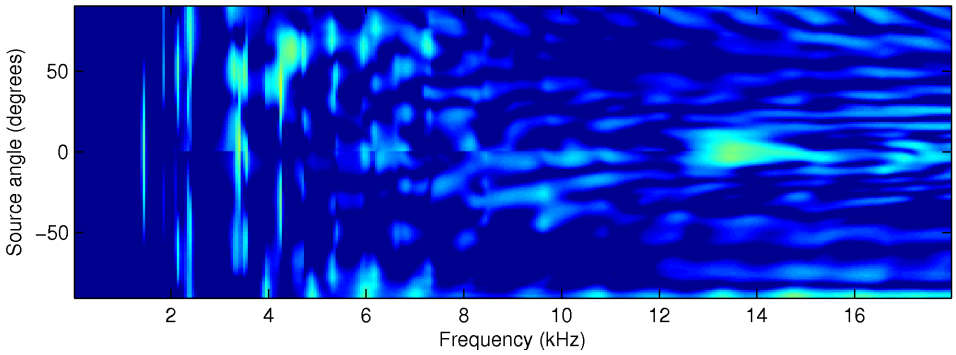


(b) Loading region restricted to depth band 0.6 to 0.7 of diameter

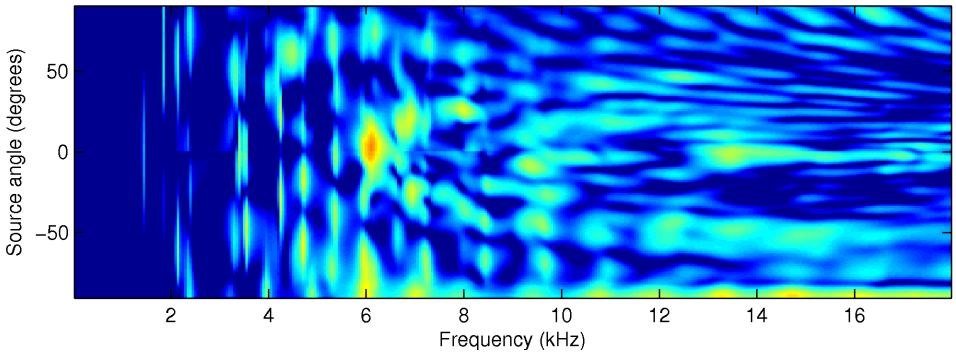


(c) Loading region restricted to depth band 0.7 to 0.85 of diameter

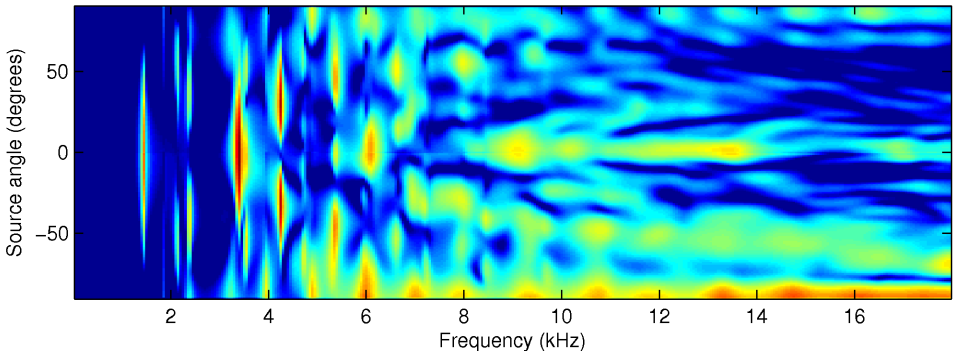


(d) Loading region restricted to depth band 0.85 to 1.0 of diameter

**Figure 7: Monostatic farfield elastic response for the pointed-end-cap shell (water-filled) with loading restricted to particular ranges of depth (described in units of height from target bottom normalized to target diameter). These correspond to the masks in Figure 6.**

angle range as in Figures 4c and d, and by restricting the loading by depth band as in Figures 7c and d. Ultimately, these findings have important implications on the feature set used by various classification algorithms. If a classifier were trained on the full range of available features then discrimination power could primarily come from features identified near broadside. This would make it impossible to distinguish between objects whose only difference is the type of filler, due to the fact that the filler has large effects on the acoustic response at angles much greater than broadside.

# 4 Simulations as a function of burial state

A major goal of this research is to understand the effects of burial depth on the target response, and eventually the implications this has on potential feature sets being used in classification algorithms. For this aspect of the research it is therefore advantageous to look at the response of the target to a fully interrogating plane wave. The target examined here is the axisymmetric pointed-end-cap water-filled shell, whose free field response was discussed in Section 3 and depicted in Figure 8 (top row). For the remainder of this report, the geometry of the simulation is represented by Figure 9. The shell is placed on (or embedded in) a flat sand sediment. The source and receiver are located 6.1 m above the sediment, at a horizontal range from the target indicated by $R$. The source/receiver travel around the target in a circular path, maintaining the same height above the sediment and range $R$ to the target, thereby simulating a circular synthetic aperture sonar (CSAS) operation. The grazing angle of the sound incident on the target is given by $\theta_g$. For a particular location of the source/receiver along the CSAS path, $\phi$ is defined to be the azimuthal rotation angle in the x-y plane. The angle of incidence $\phi_{cyl}$ is defined as the angle between the incoming wave vector and the normal to the shell surface $\hat{r}_{cyl}$ and is specifically confined to a plane defined by the incoming wave vector, and the target unit vectors $\hat{r}_{cyl}$ and $\hat{z}_{cyl}$. Figure 9 gives an example of these vectors and angles for a specific source/receiver position marked by the red 'X', corresponding to $\phi = -90$ deg. In this case, $\hat{r}_{cyl}$ happens to coincide with the z-axis. For a detailed derivation of the relationship between $\hat{r}_{cyl}$, $\theta_g$, $\phi_{cyl}$, and $\phi$ consult Appendix A in Ref. [2].

Before moving onto the burial depth analysis, it is important to illustrate the changes that occur in the shell's response due to the source/receiver now having a vertical offset from the shell (so a non-zero grazing angle). The free field response, previously depicted in Figure 8, is replotted in Figure 10 over the entire 360 deg angle range, simulating what would be observed for a complete CSAS run with $\theta_g = 0$ deg. Figure 10 shows the free field response that results from the source/receiver having the configuration depicted in Figure 9, specifically with $\theta_g = 37.3$ deg., but with no sediment present yet. The significance of having a non-zero grazing angle is such that the angle of incidence $\phi_{cyl}$ is no longer equal to the azimuthal rotation angle $\phi$. In order to couple into resonances previously observed in the free field response, the source/receiver must be at a different azimuthal rotational angle in order to achieve the required angle of incidence. This manifests in the acoustic template in two ways. The first of these is that resonances appear to move to different locations in the angle domain. The second is that many resonances observed in the free field response are no longer achievable due to the limited range in $\phi_{cyl}$ that results from having a non-zero grazing angle. The most dramatic example of this is seen in comparison of the responses when the source points directly at the nose (-90 degrees) or the flat end cap (90 degrees) of the shell. The bright, periodic resonances observed here in Figure 10 (left) require that the source direction points exactly down the axis of the shell. For non-zero grazing angle, this exact end-fire orientation can never be realized and thus these types of resonances are no longer excited. The effects of the grazing angle are studied in more detail in Section 5.

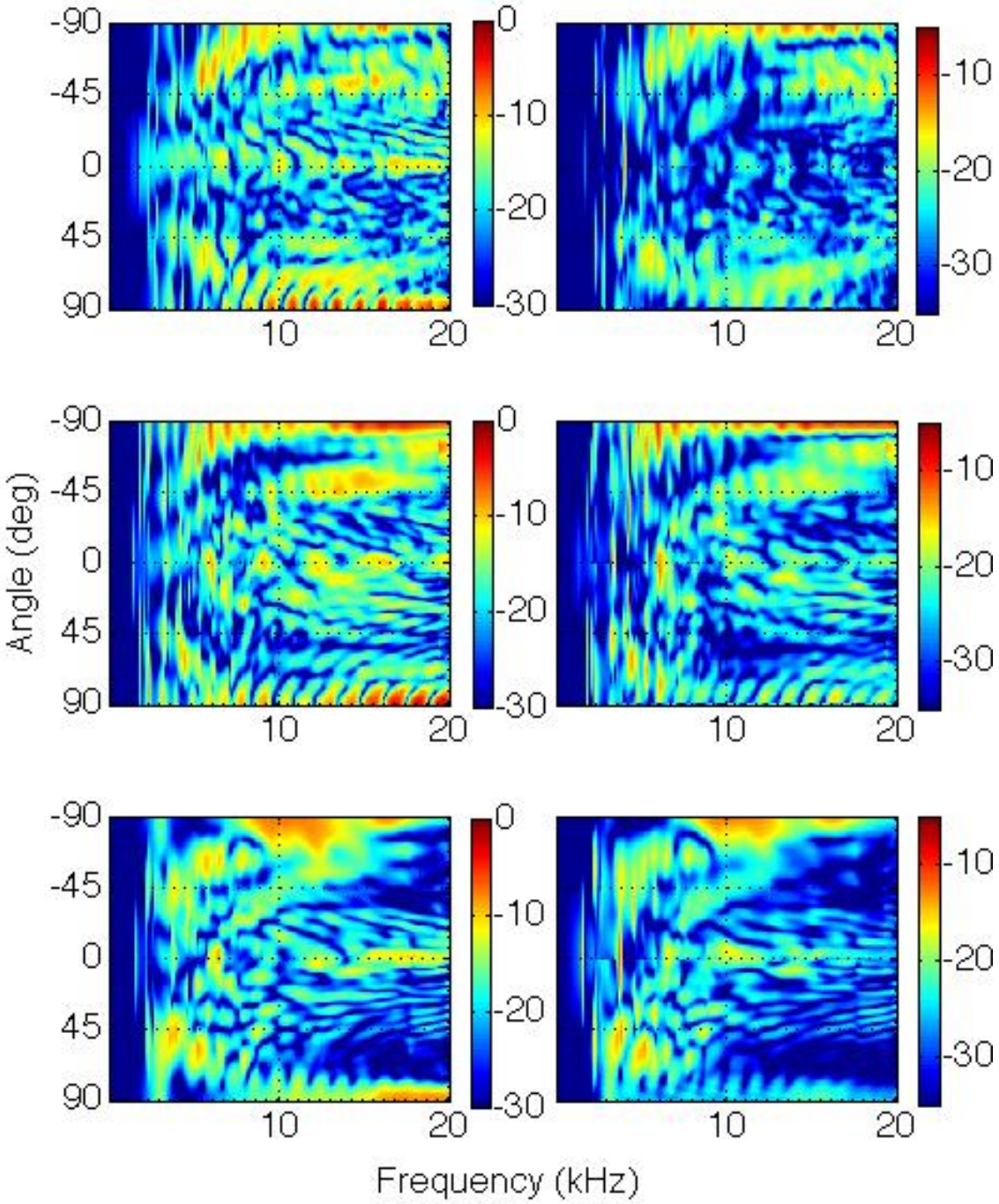


**Figure 8: Free field response of the pointed-end-cap shell constructed of steel, filled with water (top row), compared to the response of the same pointed-end-cap shell constructed of aluminum and filled with water (middle row) and air (bottom row). The right column represents the elastic response of the shells, while the left column is the response to a fully interrogating plane wave.**

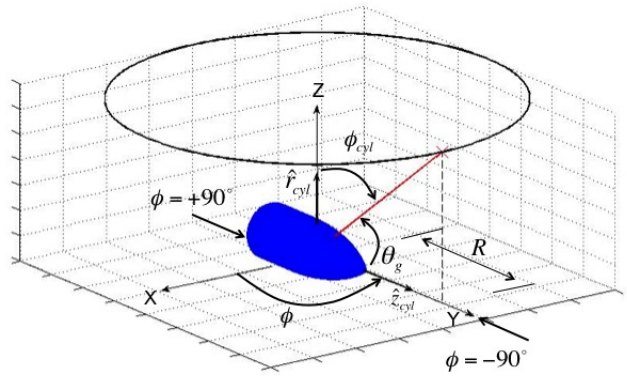


**Figure 9: Geometry associated with the circular synthetic aperture sonar (CSAS) experiment simulated in the remainder of this report.**

We consider now the effects that burial depth has on the shell's response. Figure 11 shows the response of the shell to a fully interrogating plane wave for the case of $R = 8$ m, resulting in a grazing angle $\theta_g = 37.3$ degrees. These acoustic color plots are now shown for an entire 360 degree region, representative of a complete circular path around the shell. The shell transitions from sitting proud on the sediment (left-most plot) to being completely buried (right-most plot), the titles on each of the plots indicating the specific burial depth. The effect that the presence of the sand interface has on the shell's response is understood by comparing the left-most plot in Figure 11 to the free field (of the identical $\theta_g = 37.3$ deg.) case of Figure 10. The overall response of the shell gets much stronger, specifically the resonances observed from 3 - 7 kHz, extending from +/- 60deg to +/- 120 deg. Even more striking is how much the frequency response of the shell changes near +/- 90 deg. These changes in the acoustic response are due to the existence of a boundary-reflected incident wave as well as a boundary-reflected scattered field, which are a direct result of the presence of the sand interface. These effects are discussed in more detail in Section 6. An important conclusion to emphasize here is that as the burial depth increases, as illustrated in Figure 11, the boundary-reflected paths disappear and the target's response slowly starts to resemble that of the free field response. This is illustrated in Figure 12, in which the target strength at broadside for a few of the different burial states is plotted. The fully buried case (blue dashed line) almost lies exactly on top of the free field case (black line) for frequencies less than 7 kHz. Above 7 kHz it follows the general trend of peaks and nulls, but admittedly is different in absolute TS levels. This is due to the fact that higher frequency sound will be more heavily attenuated in the sand. The free field simulation was run for the shell in water, and hence does not capture this attenuation that is present when the shell is embedded in sand.

# 5 CSAS Simulations Over a Wide Range of Grazing Angle and Environment Properties

Equally important as burial depth are the effects to the acoustic response of a target due to the grazing angle of incident sound. Recent research illustrated the large effect that the incident plane

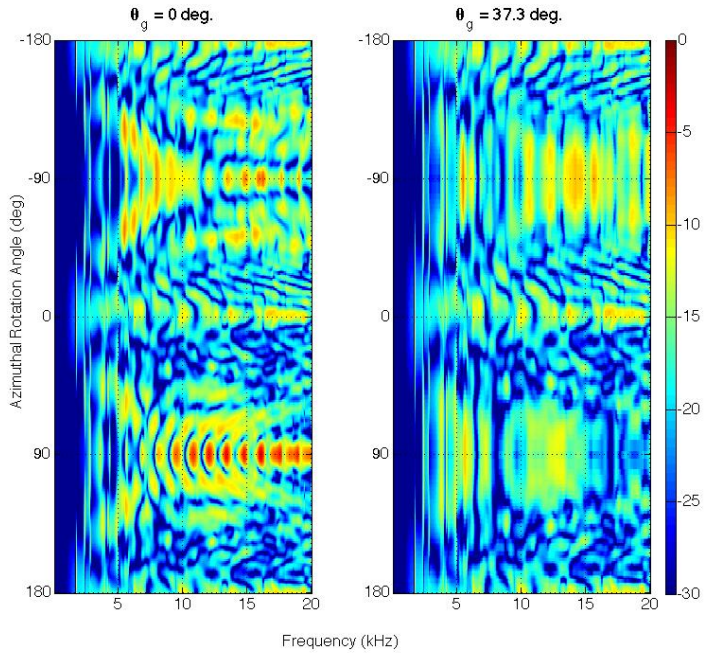


**Figure 10: Response of the pointed-end-cap, water-filled, steel shell to a fully interrogating plane wave in the free field for $\theta_g = 0$ deg. (left) and $\theta_g = 37.3$ deg. (right).**

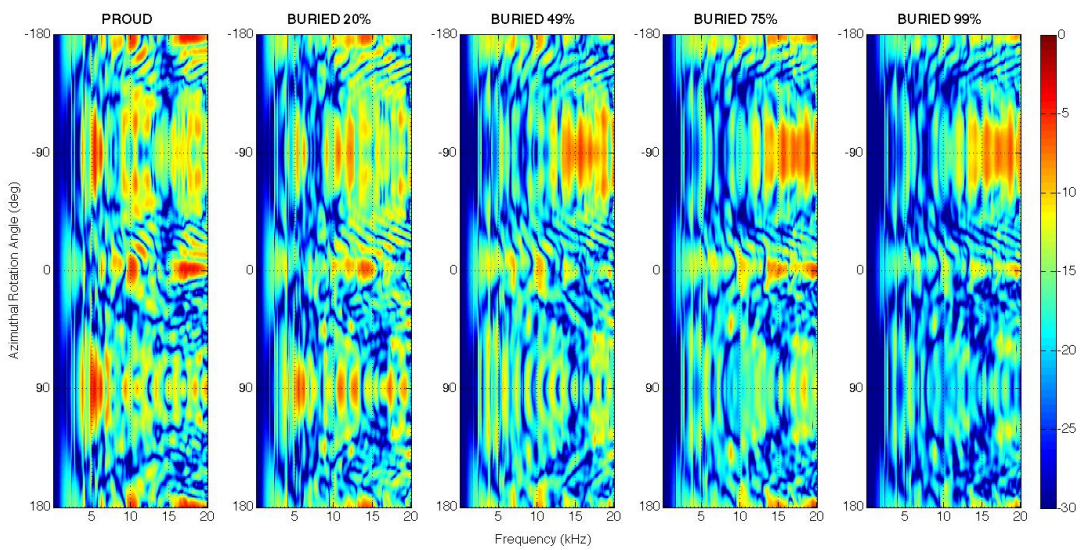


**Figure 11: Response of the pointed-end-cap, water-filled, steel shell to a fully interrogating plane wave, as it transitions from a proud configuration on a sand sediment (left) to being fully buried within the sediment (right).**

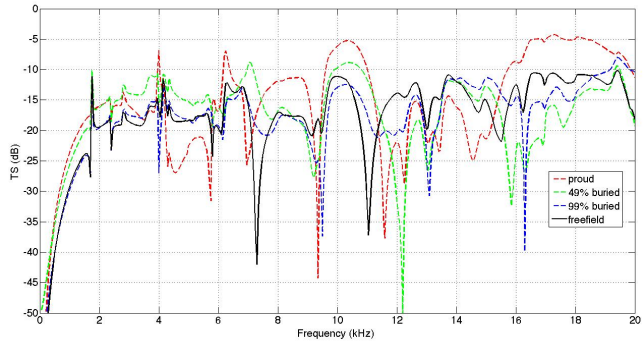


**Figure 12: Absolute target strength as a function of frequency for the pointed-end-cap, water-filled, steel shell, broadside to a fully interrogating plane wave for various burial states: proud (red dashed line), 49% buried (green dashed line), 99% buried (blue dashed line), and the free field $\theta_g = 37.3$ deg case (black line).**

wave grazing angle has on a target's acoustic response, and introduced the notion that there exists an ideal range (or grazing angle) that a vehicle would want to operate at in order to excite the strongest response from a particular type of target [11]. The research, conducted by Dr. Steve G. Kargl and funded in part under SERDP MR-1665 and MR-2231, saw the development of a fast ray model that allows for quick simulations of proud targets in an underwater environment, over a wide range of bottom types and vehicle operating scenarios (linear vs. circular SAS, steep or shallow grazing angle, etc.). Performers under this current SEED project have worked closely with Dr. Kargl in order to ensure that the component isolation/masking technique can be easily ported into the fast ray model. The concept behind this technique is that a radiated acoustic signature from a loaded target can be converted into a far field directivity pattern. This directivity pattern can then be introduced into the fast ray model as a scattering amplitude for the target, thereby allowing for the generation of acoustic color templates in a fraction of the time as compared to an FE computation. Modifications were made to the component isolation/masking code such that it can now be used to compute the scattering amplitude on a hemisphere of points surrounding a target, as required by the fast ray model. The successful merging of these two models is demonstrated in the context of the water-filled, steel shell discussed in previous sections. The shell is placed proud on a flat bottom with sound speed ($c_s$) varying from 1464 m/s (mud) to 1764 m/s (hard sand). The grazing angle ($\theta_g$) of the incident sound varied from 57 deg down to 11 deg. Results are shown in Figure 13 for a fully interrogating plane wave and Figure 14 for the elastic component, which was achieved using the fluid load technique discussed in previous sections. For both of these, the scattering amplitude required by the fast ray model was computed using the FE component isolation model developed in this SEED project. The left column corresponds to the steep grazing angle of 57 deg. and becomes smaller as you transition to the right, ending at 11 deg. for the far right column. Similarly, the top row corresponds to a sound speed in the lower medium of 1464 m/s (mud) and becomes larger as you transition down in row to a final value of 1764 m/s for the bottom row (hard sand). The first observation is that for steeper grazing angles (greater than 37 deg.), the frequency content and target strength levels tend to be constant over the full range of $c_s$ values. The implication this has in terms of classification algorithms is that under this steep grazing angle, target-centered CSAS operation, it is possible that a particular classifier trained in one specific environment could be successfully used in other environments. Secondly, the lower grazing angles (less than 20 deg.) tend to produce the maximum response from the target over

the full range of bottom types. Hence, in terms of the detection of proud targets, operating at a grazing angle less than 20 deg. would be the ideal scenario for this type of target.

It is important to note that while it may be true that operation at certain grazing angles can result in a target response that is relatively stable for bottom types ranging from mud to hard sand, the same type of invariance is not observed as a function of grazing angle. This is evidenced by the fact that in Figures 13 and 14, no matter what type of bottom the target is in contact with, the response changes drastically as you move across the page from left to right, representing a decrease in grazing angle from 57 deg. to 11 deg. The study conducted here focused on CSAS operation in the idealized case in which the target was at the center of the vehicle path, and hence the grazing angle was fixed for the complete 360 deg operation. In practice this may not be the case, and this changing grazing angle will greatly affect the measured acoustic response. Therefore, no matter what classification algorithm is implemented, the feature set must include responses from multiple grazing angles in order to have any hope of correctly distinguishing targets from clutter, and eventually distinguishing specific differences between target material and filler.

# 6 Dissecting the Effects of Multipath

In addition to being able study the target's response over a wide range of grazing angle and environment properties, the fast ray model also allows the investigation of the contributions of individual ray paths, which is a key tool when trying to interpret the physical mechanisms associated with the various resonances in the acoustic color. Dissecting the ray paths has been the subject of resent work by performers and collaborators of this project (see for example [2, 3, 11, 12]). The ray paths are illustrated in Figure 15 and correspond to a direct path (path 1), a bistatic path which involves one bounce off the interface either before or after the target interaction (paths 2 and 3 respectively), and a double bounce path (path 4) in which the sound reflects off the interface both before and after interaction with the target. Figure 16 illustrates how the different path contributions drive the full response for the specific case of the shell proud on a sand sediment ($c_s = 1704$ m/s) with $\theta_g = 37.3$ deg. The left panel is the sum of all paths, middle left is the path 1 contribution, middle right is the sum of paths 1 and 4, and the right plot is the sum of paths 2 and 3. We can see that paths 1 and 4 tend to drive the shell's response around +/-90 deg from about 3-6 kHz, and some of the higher frequency resonances observed around -90 deg from 15-20 kHz. The bistatic paths 2 and 3 drive more of the middle frequency range (7-15 kHz) around -90 deg, and nearly the full frequency range (6-20 kHz) around 90 deg. All of this becomes even more clear by examining just the elastic component of these multipath contributions, given in Figure 17, and arrived at using the fluid front loading mask.

As was the case for the full response of the shell, the multipath contributions will also be highly dependent on grazing angle. To illustrate this, the elastic response for the path contributions for the case of $\theta_g = 11$ deg is given in Figure 18. In this situation, the path 2 and 3 contributions tend to drive the shell's response over much of the entire template. This tells us that at these shallower grazing angles, the shell tends towards radiating a lot of energy off in directions other than backscattering. The presence of the sand and the nature of these resonances affords us an enhanced response in the backscattering direction that would otherwise not be visible.

# 7 Implementation of Component Isolation Techniques

In this last section, an example is given that shows how the analysis and techniques of the previous sections can be combined to help isolate various components making up the physical response of

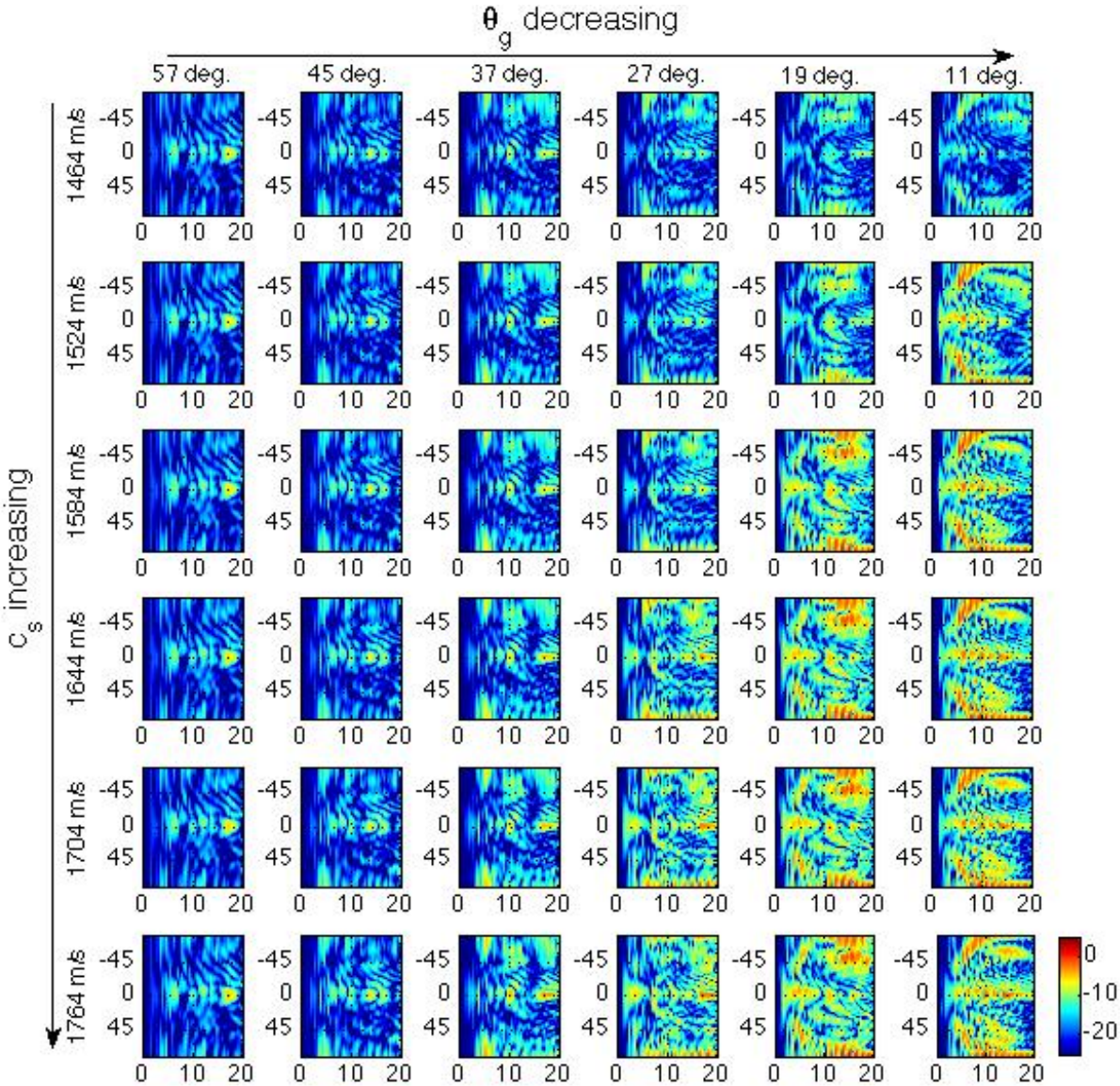


**Figure 13: Response of the pointed-end-cap steel, water-filled shell, proud on a flat medium of varying sound speed and density, and subjected to fully interrogating plane waves from different grazing angles. Each column is a specific $\theta_g$, the first column on the left corresponding to $\theta_g = 57$ deg., and decreases as you move across the page to the right to a value of $\theta_g = 11$ deg. Meanwhile, each row is a fixed $c_s$, the top row corresponding to $c_s = 1464$ m/s (similar to mud), and increases as you move down the page to $c_s = 1764$ m/s (hard sand). The x-axis is frequency in kHz and the y-axis is $\phi_{cyl}$ in degrees (see Fig. 9). To facilitate better viewing, the results from only 180 deg. of the CSAS path is shown.**

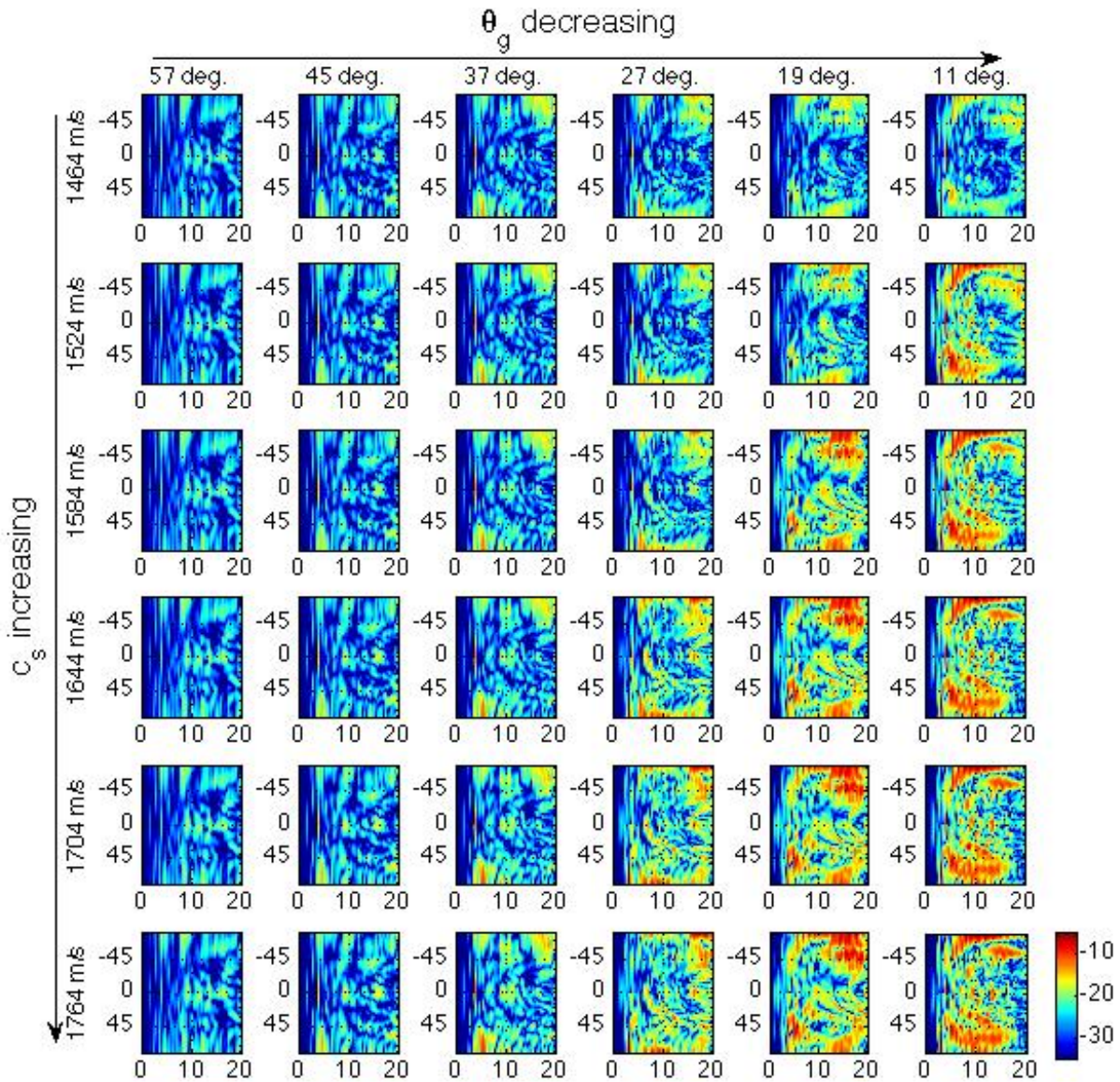


**Figure 14: Elastic only response of the pointed-end-cap steel, water-filled shell, proud on a flat medium of varying sound speed and density, and varying incident grazing angles. Each column is a specific $\theta_g$, the first column on the left corresponding to $\theta_g = 57$ deg., and decreases as you move across the page to the right to a value of $\theta_g = 11$ deg. Meanwhile, each row is a fixed $c_s$, the top row corresponding to $c_s = 1464$ m/s (similar to mud), and increases as you move down the page to $c_s = 1764$ m/s (hard sand). The x-axis is frequency in kHz and the y-axis is $\phi_{cyl}$ in degrees (see Fig. 9). To facilitate better viewing, the results from only 180 deg. of the CSAS path is shown.**

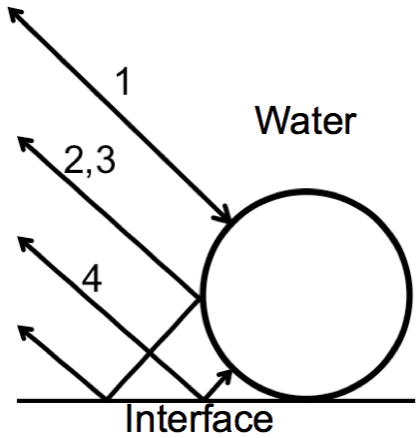


**Figure 15: Illustration of the individual ray paths resulting from the presence of the interface [2, 12]. Path 1 is the direct path, paths 2 and 3 take one bounce off the interface, either before or after interacting with the target, and path 4 is the double bounce path in which the sound hits the interface both before and after interacting with the target.**

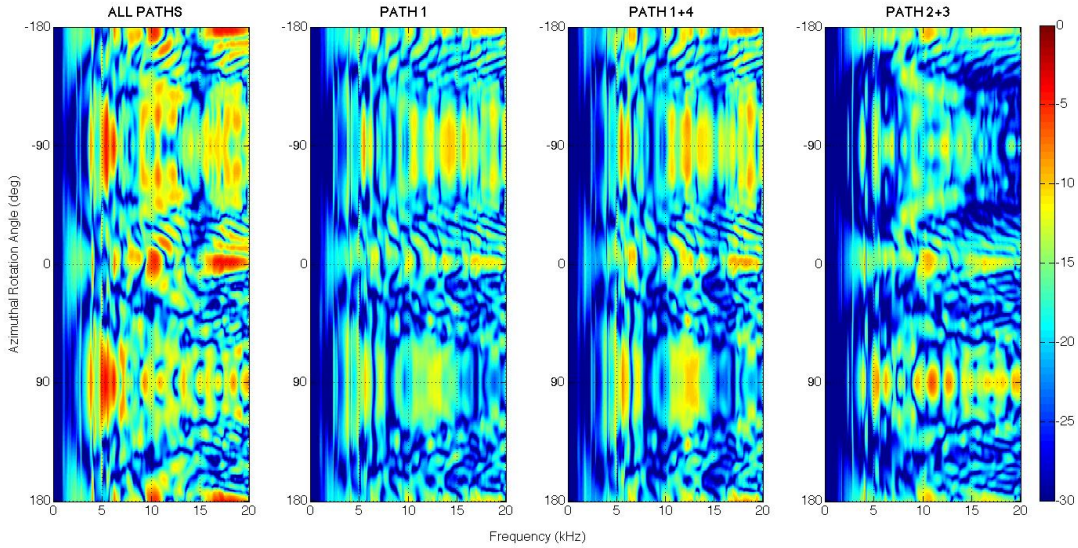


**Figure 16: Individual path contributions for the full plane wave response of the pointed-end-cap, water-filled, steel shell, proud on a sand sediment (sound speed = 1704 m/s), with incident grazing angle $\theta_g = 37.3$ deg.**

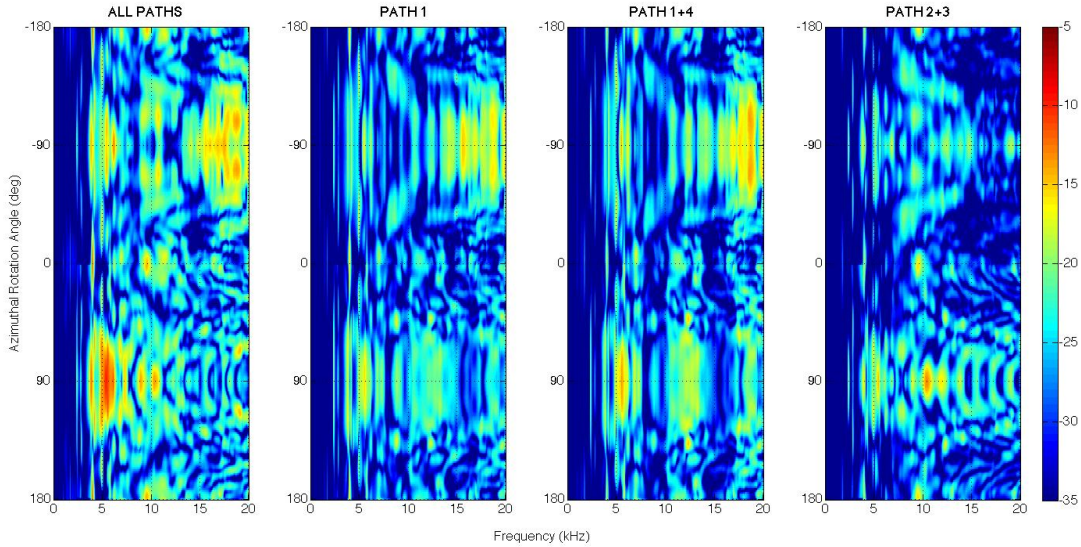


**Figure 17: Individual path contributions for the elastic response of the pointed-end-cap, water-filled, steel shell, proud on a sand sediment (sound speed = 1704 m/s), with incident grazing angle $\theta_g = 37.3$ deg.**

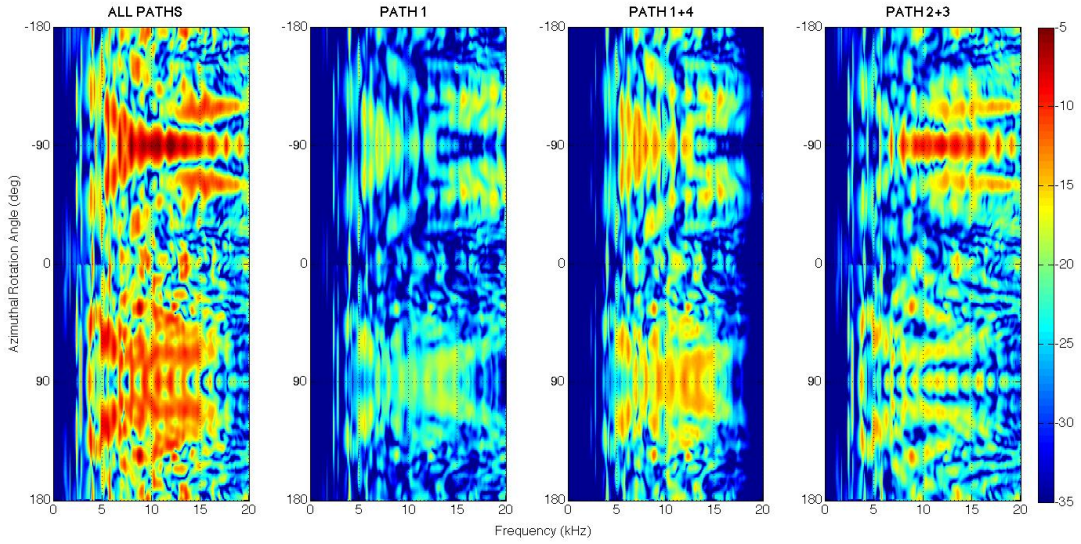


**Figure 18: Individual path contributions for the elastic response of the pointed-end-cap, water-filled, steel shell, proud on a sand sediment (sound speed = 1704 m/s), with incident grazing angle $\theta_g = 11$ deg.**

a target. In what follows, knowledge gained from the studies conducted on filler, burial depth and grazing angle, are combined with the techniques of isolating individual path contributions, the elastic response and a specific coupling region on the target. The specific example being dissected here is the response of the water-filled, steel shell to a fully interrogating plane wave with $\theta_g = 33.7$ deg, in a 99% burial state in the sand sediment ($c_s = 1704$ m/s). These results were given in Figure 11 and are replotted in the left most plot of Figure 19. In Section 4 we learned that in the case of steep grazing angle and full burial, the shell response begins to resemble that of the free field response, albeit with some differences due to the fact that the free field computation was done in water, and hence does not contain the appropriate attenuation that would be present were the shell surrounded by sand. This free field response was plotted in Figure 10, but it can just as easily be attained by examining the individual path contributions for the proud simulation of identical grazing angle. The path 1, or direct path, contribution in Figure 16 is simply the free field response of the shell, and is replotted here in the middle left plot of Figure 19. As illustrated throughout this report, an advantageous way of loading the shell is using the fluid front load technique, which isolates the elastic component. The path 1, elastic response is given in the middle right plot of Figure 19. Although this particular plot was discussed previously in Section 6, some important observations can be made by comparing it here next to the full response of the completely buried shell. By removing the rigid component it can be observed that the response of the shell near the nose (-60 to -120 ) and near the tail (60 to 120) in this proud-path 1 situation starts to resemble that of the fully buried case. We know from Section 3 that these are the areas of the template that are heavily driven by the particular filler inside of the shell. We can go a step further and drive a number of these resonances by applying a region-loading mask as in Section 2.1 that restricts the coupling of the incident wave to the angular region 45 - 55 deg, which is shown in the right most plot of Figure 19. For example, this isolates the resonances observed near -40 deg from 7-10 kHz, various resonances at 45 deg in the region from about 9-13 kHz, and +/-60 to 70 deg from 18-20 kHz, just to name a few. Ultimately, this section illustrated just one example in which a simple free field computation, coupled with the various component isolation techniques presented here, can serve to isolate specific features of the template that are observed not only in the free field, but also as the target transitions from proud to completely buried.

# 8 Future Work

The goal of this SEED effort was to demonstrate a proof-of-concept for the value of isolating the contribution of various aspects of the physics contributing to a complex elastic respons of a target. In this work, we loaded particular regions of the target as a method for better understanding the full-physics response and the way in which this response will vary with environment and target conditions. The infrastructure developed in the completed effort and the results obtained suggest a number of directions we propose to pursue which we believe will allow a much deeper understanding of relevant features and how those features contribute to automatic classification performance. We are collaborating in-house with Kevin Williams and Steve Kargl, who are funded separately by SERDP and ONR, to focus our proposed research on the ultimate goal of automatic and operator-assisted target classification. The block diagram in Figure 20 shows the data flow of the classification system we are targeting, with general block names and specific current implementations shown in parentheses. Although this type of system has shown satisfactory results on limited real data tests, very little of our understanding of target physics has gone into its design or block selection.

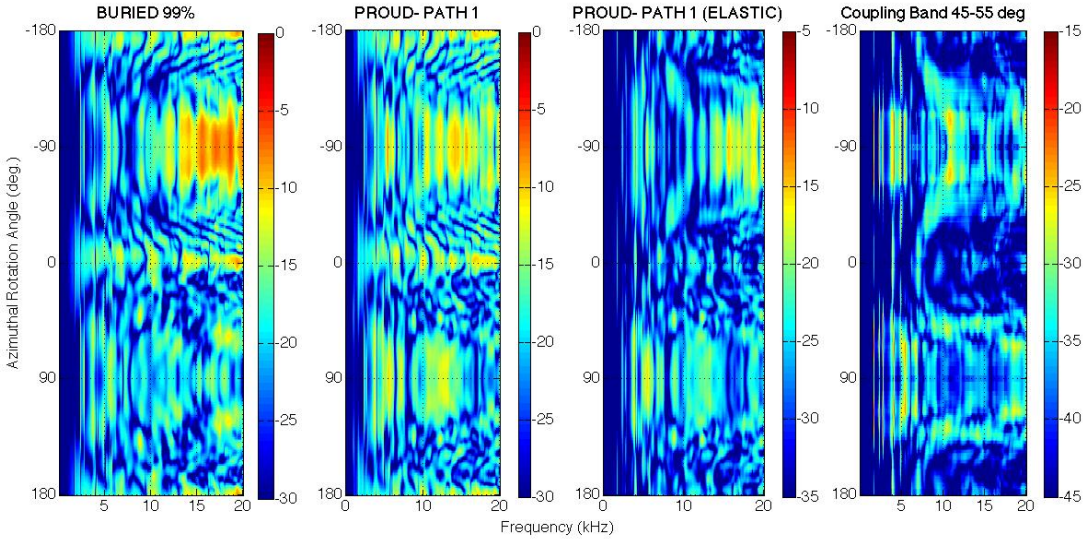


**Figure 19: Application of the component isolation techniques to the pointed-end-cap, water-filled, steel shell, completely buried in a sand sediment ($c_s = 1704$ m/s). The left plot is the shell's response to a fully interrogating plane wave ($\theta_g = 37.3$ deg) while it's completely buried in sand. The middle-left plot shows the full response for the path 1 contribution when the shell is proud on the sand, while the middle-right is just the elastic component. The right plot is the elastic component of the the free field ($\theta_g = 37.3$ deg.) response where the incident waves are restricted by an appropriate mask to the coupling angle band of 45 to 55 deg.**

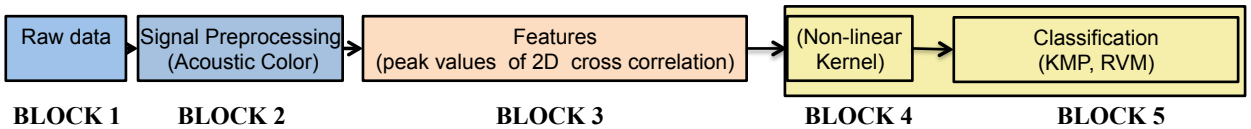


**Figure 20: Block diagram of baseline classification system for SERDP MR-2505 (Kargl) and follow-on ONR proposal to Kyle Becker (Williams). Although this system has provided reasonable performance on some datasets, the signal preprocessing and feature extraction are very generic and the goal of the proposed work is to develop physically-motivated improvements to Blocks 2 and 3. See Kargl's SERDP Scientific Advisory Board presentation for more details on this system.**

In the proposed work, we will use FE techniques to model targets with important similarities to munitions. Our approach allows us to isolate the physical sources of the individual components making up the complex target response. By simulating these in isolation we will be able to assess their contribution to automatic classifier performance, and predict the change in this performance as a function of burial state. Finally, we will validate the conclusions of this study by manufacturing targets which will be studied in (separately funded) sea trials.

**Modeling:** As described in this report, we will use the COMSOL FE modeling environment to create simulations of targets whose behavior will be relevant to the target types of interest. Models developed under the current SEED effort are parameterized to be easily configured for a wide variety of shapes, sizes, and materials. In addition, the model outputs can now be easily ported into the fast ray model developed by Dr. Steve G. Kargl under SERDP MR-1665 and MR-2331. In later years of the project we may take advantage of further advances (under independent development) to include more complicated targets.

**Physics Decomposition:** Using the infrastructure developed and tested in the current SERDP SEED effort, and the techniques described in the Appendix A and in our published work [1], we will decompose the full-physics response of research targets of interest using a variety of methods, thus enabling the study of individual components making up the target response. The ultimate goal of this work is to adapt the generic signal processing and feature extraction in Blocks 2 and 3 of Figure 20 to incorporate our knowledge of the physics of signature generation. The infrastructure developed under the SEED work allows us to decompose the structure by:

- separately modeling elastic and inelastic components
- further decomposition of the elastic response by wave behavior and influence of filler material. The six nearfield pressure maps shown in Figure 5 show the effects of multiple different wave types, many of which can be isolated by further manipulations of the physics. For example, we can restrict waves to radial travel or axial travel, or even to helical paths, and to surface or deeper movement. This will allow us to definitively understand the components of the full return in terms of the isolated simpler wave behaviors and their interactions.
- separately modeling the multipath effects of the sediment interface, leveraging the fast ray model developed by Dr. Kargl under SERDP MR-1665 and MR-2331.

**Target Shape/Material Analysis:** We will also consider the effects of shell and filler material on the components thus isolated (see Figure 8). We can use the physics-isolation approach to separately consider the effects of filler on shell-borne waves and the travel of energy through the filler itself. In particular, we will look at the subsurface behavior (stress and displacement) of the target to understand the relationship between the features in the external field and the shell thickness and filler material.

**Burial Effects Analysis:** The mechanisms isolated in the decompositions above can be more easily modified to account for burial state and sediment type than can the complex full-physics response. Continuing with the same work as described in the Target Identification Analysis above, we will assess performance as a function of: burial of coupling/reflection surfaces, damping of surface waves, and sediment-reflected multipath effects on coupling surface locations. Effects of the individually-manipulated mechanisms will be compared to modeled effects on full-physics burial

cases, and additional effects will be assessed as necessary.

**Target Identification/Classification Analysis:** Researchers at APL-UW [13, 14] and elsewhere (including [15, 16]) have developed empirically tested systems for automatic identification of acoustically interrogated targets resting on the sea floor. We will adapt the system outlined in Figure 20 for the purpose of evaluating the physical mechanisms isolated in the decomposition above. We note specifically that the approach we propose offers insight beyond the standard FE approach because by comparing identification performance on signatures with and without particular physical mechanisms activated, we can assess their importance in system performance. In addition to the assessment of the importance of the physical mechanisms described above, this analysis approach will enable us to provide guidance on different interrogation scenarios, including comparison of the value of various side-looking versus look-down setups, and the features utilized by each.

**Sea Trial Validation:** In follow-on proposals to active APL-UW programs sponsored by SERDP and ONR under Investigators Dr. Steve Kargl and Dr. Kevin Williams, shallow-water tests are planned for FY16. Partial funds for the sea trial have been secured through SERDP MR-2505, and assuming the follow-on ONR proposal is funded, we will manufacture a target or targets which will be included in those trials at no cost. This will enable validation of the models developed and assessed over the course of the project.

The follow-on work described above would be a three-year effort at $150k in year 1 and $200k in years two and three. A suggested schedule is shown below, with the exact timing of the (separately funded) sea trials dependent on the acquisition of joint funding from ONR, as well as the availability of ship time.

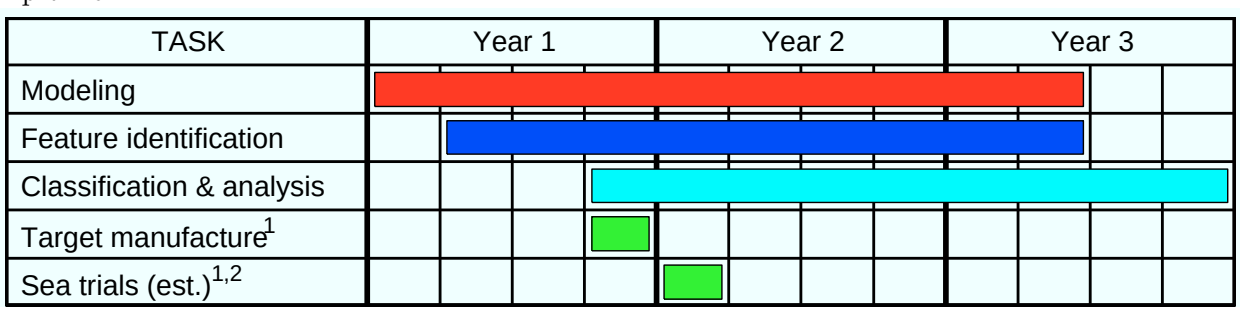


[1]Assumes sea trials [2]Funded separately by ONR and SERDP MR-2505 (Kargl).

## References


[1] Lane Owsley and Jack McLaughlin, "Modeling acoustic target response by component," in *Proceedings of MTS/IEEE OCEANS*, 2010.

[2] Kevin L. Williams, Steven G. Kargl, Eric I. Thorsos, David S. Burnett, Joseph L. Lopes, Mario Zampolli, and Philip L. Marston, "Acoustic scattering from a solid aluminum cylinder in contact with a sand sediment: Measurements, modeling, and interpretation," *The Journal of the Acoustical Society of America*, vol. 127, no. 6, pp. 3356–3371, 2010.

[3] A.L. España, K.L. Williams, D.S. Plotnick, and P.L. Marston, "Acoustic scattering from a water-filled cylindrical shell: Measurements, modeling, and interpretation," *The Journal of the Acoustical Society of America*, vol. 136, pp. 109–121, 2014.

[4] M. Zampolli, A. Tesei, F.B. Jensen, N. Malm, and J.B. Blottman III, "A computationally efficient finite element model with perfectly matched layers applied to scattering from axially symmetric objects," in *Journal of the Acoustical Society of America*, September 2007, vol. 122, no. 3, pp. 1472–1485.

[5] M.J.J. Nijhof, A. España, and K. Williams, "Efficient calculation of broadband acoustic scattering from a partially, obliquely buried cylinder," *Proc. 1st International Conf. Exhibition Underwater Acoustics*, pp. 697–702, 2013.

[6] M. Zampolli, A. L. España, K. L. Williams, S. G. Kargl, E. I. Thorsos, J. L. Kennedy J. L. Lopes, and P. L. Marston, "Low- to mid-frequency scattering from elastic objects on a sand sea floor: Simulation of frequency and aspect dependent structural echoes," *Journal of Computational Acoustics*, vol. 20, no. 2, 2012.

[7] F.J. Blonigen and P. L. Marston, "Leaky helical flexural wave scattering contributions from tilted cylindrical shells: Ray theory and wave-vector anisotropy," *The Journal of the Acoustical Society of America*, vol. 110, pp. 1764–1769, 2001.

[8] S. F. Morse and P. L. Marston, "Meridional ray contributions to scattering by tilted cylindrical shells above the coincidence frequency: ray theory and computations," *The Journal of the Acoustical Society of America*, vol. 106, pp. 2595–2600, 1999.

[9] Steven G. Kargl and Philip L. Marston, "Observations and modeling of the backscattering of short tone bursts from a spherical shell: Lamb wave echoes, glory, and axial reverberations," *The Journal of the Acoustical Society of America*, vol. 85, no. 3, pp. 1014–1028, 1989.

[10] P. L. Marston S. F. Morse and G. Kaduchak, "High-frequency backscattering enhancements by thick finite cylindrical shells in water at oblique incidence: Experiments, interpretation, and calculations," *The Journal of the Acoustical Society of America*, vol. 103, pp. 785–794, 1998.

[11] S. Kargl, A. L. España, K. Williams, J. L. Kennedy, and J. Lopes, "Scattering from objects at a water-sediment interface: Experiment, high-speed and high-fidelity models, and physical insight," *IEEE Journal of Oceanic Engineering*, Accepted for publication Sep. 2014.

[12] D.S. Plotnick, P.L. Marston, K.L. Williams, and A.L. España, "High frequency backscattering by a solid cylinder with axis tilted relative to a nearby horizontal surface," *The Journal of the Acoustical Society of America*, Accepted for publication Nov. 3, 2014.

[13] Kevin Williams, *personal communication*, 2014.

[14] J. McLaughlin and L. Owsley, "Combined screener/classifier architectures for mine countermeasures," *Journal of Underwater Acoustics*, pp. 697–702, October 2008.

[15] Joseph A Bucaro, Zachary J Waters, Brian H Houston, Harry J Simpson, Angie Sarkissian, Saikat Dey, and Timothy J Yoder, "Acoustic identification of buried underwater unexploded ordnance using a numerically trained classifier (l)," *The Journal of the Acoustical Society of America*, vol. 132, no. 6, pp. 3614–3617, 2012.

[16] Ananya Sen Gupta, Daniel Schupp, and Ivars Kirsteins, "Dynamic target identification and classification based on resonance topography grouping," in *Proceedings of the Asilomar Conference on Signals, Systems, and Computers (to appear)*, 2014.

[17] A. Tesei, A. Maguer, W. L. J. Fox, R. Lim, and H. Schmidt, "Measurements and modeling of acoustic scattering from partially and completely buried spherical shells," *The Journal of the Acoustical Society of America*, vol. 112, no. 5, pp. 1817–1830, 2002.

# Appendices

## A Physics feature Isolation: Specular, Inelastic Fluid-Borne, and Elastic

APL-UW has used COMSOL to develop solid/acoustic FE models for underwater elastic targets interrogated with acoustic energy[1]. For a complete representation of the physics a researcher would model the pressure field created by the interrogating source as $p_{inc}$. The scattered response is $p_{scat}$, so it follows that the total acoustic pressure field is $p_{tot} = p_{inc} + p_{scat}$. In the example described below, if we model the physics of the full empirically testable scenario, $p_{inc}$ ( the incident pressure wave) is a plane wave traveling in the negative-$y$ direction. The example described in this appendix is a spherical shell for which we have tank-collected results from the Naval Research Laboratory (NRL) for comparison.

When we simulate the complete physics of the spherical shell interrogated with a plane wave, the pressure appears as a fluid load on the exterior boundary of the shell:

$$\mathbf{F} = -p_{tot}\mathbf{N}, \tag{5}$$

where $\mathbf{N}$ is the outward-facing normal for each point on the exterior of the shell. The solid mechanics physics of the shell's interior are then coupled back into the water by the constraint that the normal component of the water acceleration be equal to that of the solid acceleration at every point on the solid-fluid interface:

$$\mathbf{a}_{fluid} \cdot \mathbf{N} = \mathbf{a}_{solid} \cdot \mathbf{N}. \tag{6}$$

Given these straightforward equations and appropriate boundary conditions (including perfectly matched layers (PMLs) [4] at the exterior of the modeled water to prevent reflection of the scattered wave), we produce an estimate of the scattered response which matches to a high degree of fidelity with the analytic solution [17] and with data collected in freefield tank experiments at NRL, including phenomena which are interpreted as specular response, resonant components, and surface-guided fluid-borne waves. A cartoon representation of this full-physics model is shown in Figure 21a. We view modeling of individual physical mechanisms contributing to the complete response as a process of turning off particular manifestations of the incident pressure wave or of the physics representation of the geometry itself.

The most straightforward restriction is that which produces the inelastic response. In this case, as represented in Figure 21b, we fix the solid-fluid interface acceleration

$$\mathbf{a}_{fluid} \cdot \mathbf{N} = 0 \tag{7}$$

which is, of course, the inelastic condition and results in an estimate of the specular and other fluid-borne components of the response. It is noted that this is in fact an overestimate in the sense that it assumes no energy is transferred into the target object.

Further separation of the inelastic response can be achieved by isolating the specular component. For the monostatic case, this is done, as shown in Figure 21c, by adding PMLs that absorb waves being guided around the object and leaving only those that bounce off the target and return directly to the receiver. The user can then isolate the surface guided component by subtracting the specular pressure field from the inelastic pressure field.

FE modeling allows for a wide range of possibilities for isolating portions of the elastic response. The basic paradigm developed at APL-UW is to stimulate the internal movement directly rather

than as some effect of incident pressure in the fluid. To reproduce the entirety of the elastic response, we can reduce the forcing function only to the direct load on the target (*i.e.* by setting the incident pressure to 0) and creating a new force on the shell which is identical to that of the fluid load in Equation 5. This is illustrated in Figure 21d. An alternate approach is to restrict the region over which this force is applied (for example, to isolate a certain type of wave which theory tells us couples into the target only at certain incidence angles). This approach would allow us to simulate scenarios where a target is partially buried, and the surface available for pressure wave coupling is reduced. Other restrictions are also possible, such as turning off the physics of only a certain part of the internal structure.

**Example Model: Spherical Shell**

To illustrate the technique just outlined, we present a breakdown for the canonical spherical shell, in this case an air-filled steel shell with radius .2832 meters and shell thickness .0152 meters (dimensions corresponding to an actual target that was used for validation of the full-model simulation). In Figure 22 we show the COMSOL simulation of the full sphere response to a plane wave at 13 kHz. The simulated full-spectrum farfield response (shown in Figure 24) is extremely close to that of the tank-collected free-field spectrum.

The first component isolated is the inelastic portion, the field magnitude of which is shown in Figure 23a, simulated using the model outlined in Figure 21b. This includes both specular response and response due to waterborne waves guided around the exterior of the sphere; both can be seen and tracked in an animation of the simulated response. To separate these two, we use the PML absorber illustrated in Figure 21c to produce the result shown in Figure 23b. In this case, all waves (including shell-guided waves) that travel past the midline of the scatterer are absorbed, and only the specular response is returned. The elastic component of the response, created using the method illustrated in Figures 21d, is shown in Figures 23c and 23d (We have chosen to show two representative frequencies as the elastic component fields differ most with frequency). Some of the monostatic farfield spectra which have been compiled from a frequency sweep are shown in Figure 24.

Figure 24 shows the resulting scattered spectra in the farfield. The full and inelastic spectra correspond well with theory and data. The response for the model which isolates the elastic component is a good representation of the resonances present in the observed responses.

# B Using Table Lookups to Efficiently Simulate Acoustic Responses

It is the goal of this SEED effort to isolate components of the complex return from elastic targets, particularly focusing on how those components are affected by burial state. Much of this is accomplished empirically by observing the simulation of components arising from a variety of different loading conditions and burial states. The modeling technique used here is a hybrid finite element (FE) - propagation approach, in which the interaction of sound with the target is handled via a 2D axisymmetric FE model, while the resulting scattered pressure field is propagated in 3D to the far field using a Helmholtz integral [6]. While the propagation piece of this computation is fast, FE modeling techniques, such as those used in this project, require tremendous computational and memory resources, and this is true many times over when research involves studying the response over a wide variety of conditions as is the case in our current research. As a result, it is necessary to approach the problem systematically in order to make the use of physical and computational resources practical.

We therefore make use of FE lookup tables, a technique developed by Marten Nijhof at TNO [5]. The concept only requires the use of a FE model for the target in the free field. Within the FE computational domain, the target and surrounding medium are meshed, or broken down into small elements. Each of these elements contain $N$ of gauss points ($N$ is specified by the user, and for the models in this project is equal to 6). The gauss points are defined as the integration points within an element at which the integrals are evaluated numerically by the FE software package. The lookup tables make use of these gauss points by individually loading one-by-one the points that define the outer surface of the target, and recording the subsequent response (pressure and derivative) at the other surface gauss points.

After this table is constructed, the response of the target to any generic incident field and in any orientation within the environment (symmetric or not) can be built up from a linear combination of the appropriate lookup entries. Generation of a complete lookup table takes approximately 7 days of computation time and 1 TB of disk space on currently available platforms. As a result of this initial investment, an acoustic template for the target in a proud or buried configuration, spanning the full 180 degrees in angle range and about 20 kHz in frequency range, can be simulated in one day. In addition, we are able to restrict the physics to many different configurations and use them to model each return component's response to burial separately.

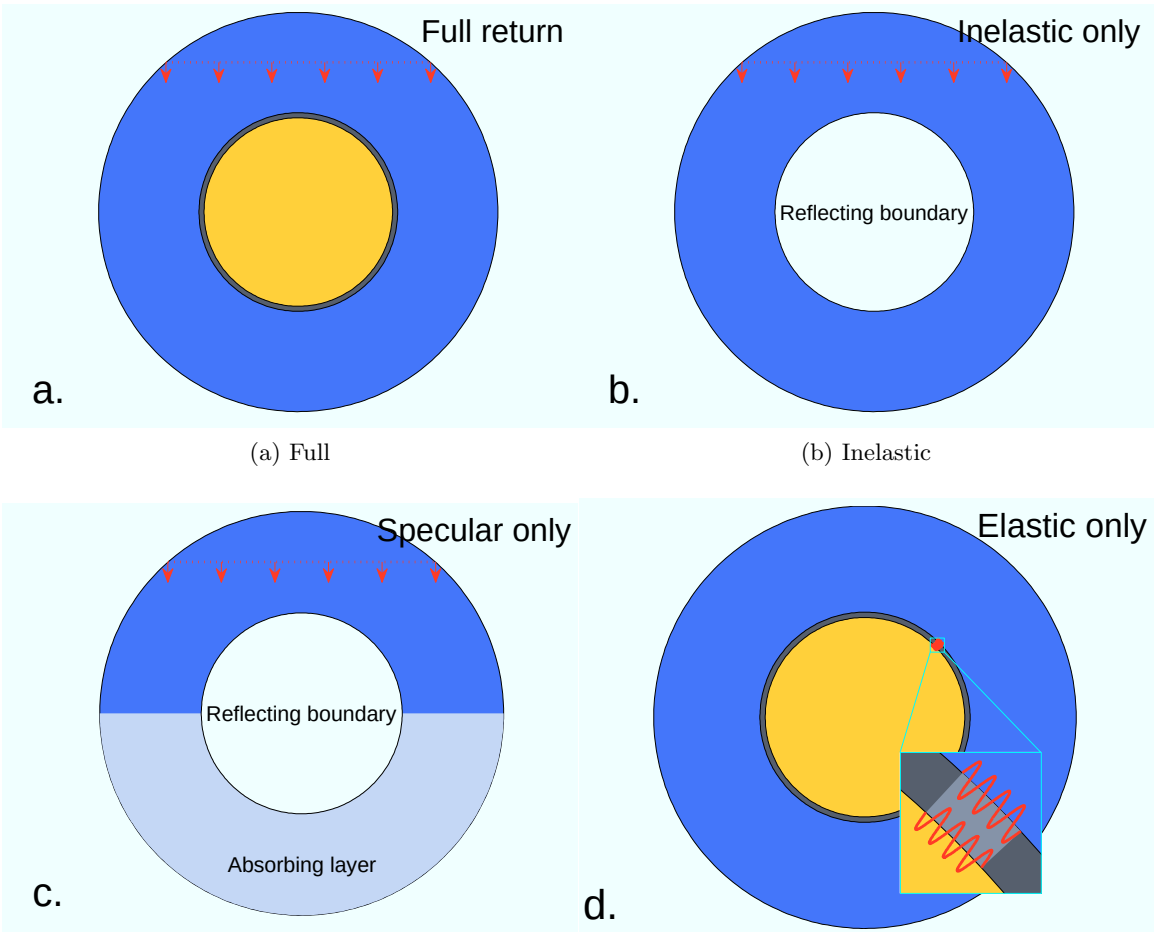


(a) Full

(b) Inelastic

(c) Specular

(d) Resonant

**Figure 21: Illustrations of some options for modeling components of the response of an elastic spherical shell to an acoustic plane wave.**

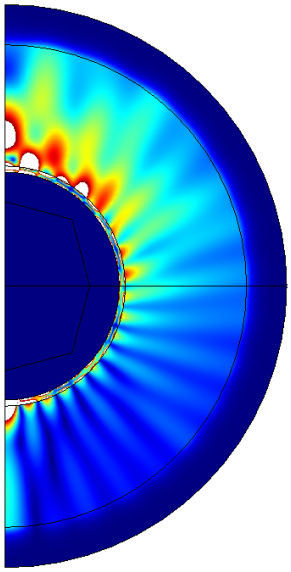

**Figure 22: The magnitude of the scattered pressure field for the full FE simulation at 13 kHz.**

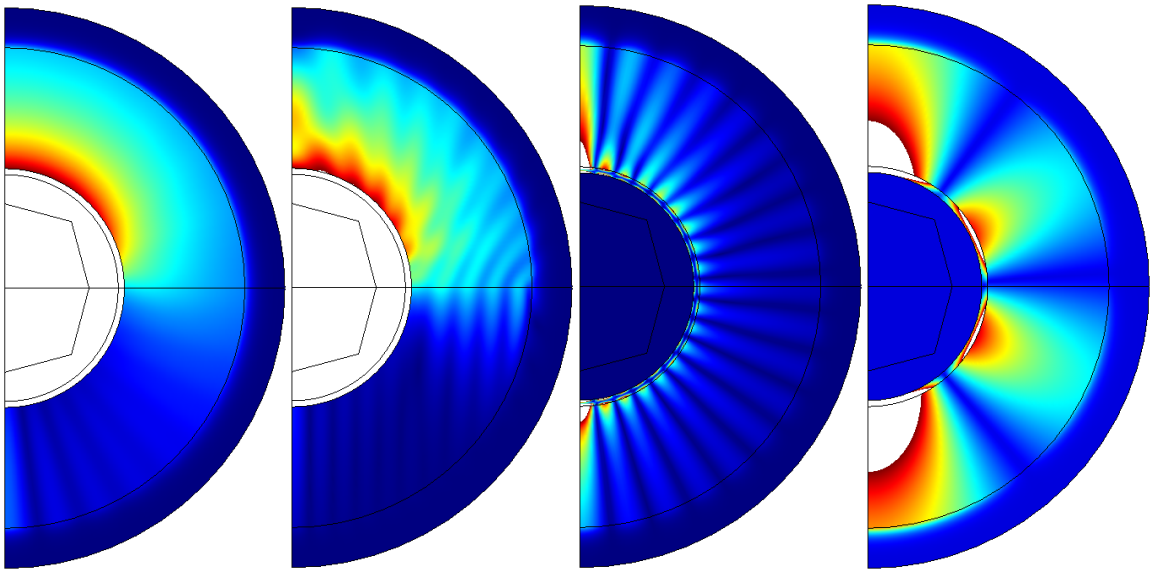

(a) Inelastic (b) Specular (c) Resonant, 13000 Hz (d) Resonant, 2344 Hz

**Figure 23: The magnitude of the scattered pressure field for the FE simulation of various components of the response.**

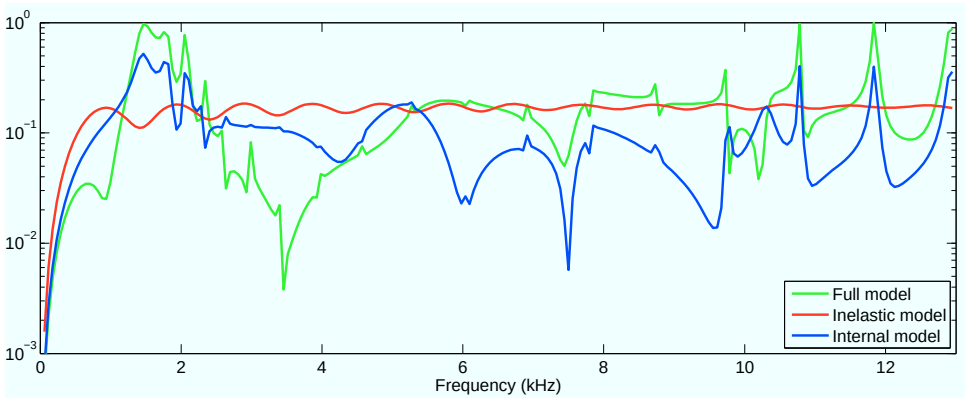


**Figure 24: Spectra of scattered responses for various component models**